Validity domain of the Benney equation including Marangoni effect for closed and open flows

By B. SCHEID[1,2], C. RUYER-QUIL[2], U. THIELE[3], O. A. KABOV[1,4], J. C. LEGROS[1] AND P. COLINET†[1]

[1]Service de Chimie-Physique E.P., Université Libre de Bruxelles C.P. 165/62, 1050 Brussels, BELGIUM
[2]Laboratoire FAST, UMR 7608, CNRS, Universités P. et M. Curie et Paris Sud, Bât. 502, Campus Universitaire, 91405 Orsay Cedex, FRANCE
[3]Max-Planck-Institut für Physik komplexer Systeme, Nöthnitzer Str. 38, D-01187 Dresden, GERMANY
[4]Institute of Thermophysics SB RAS, 630090, Novosibirsk, RUSSIA
bscheid@ulb.ac.be; ruyer@fast.u-psud.fr; thiele@mpipks-dresden.mpg.de

(Received 29 October 2004)

The Benney equation including thermocapillary effects is considered to study a liquid film flowing down a homogeneously heated inclined wall. The link between finite-time blow-up of the Benney equation and absence of one-hump travelling-wave solution of the associated dynamical system is accurately demonstrated in the whole range of linearly unstable wavenumbers. Then the blow-up boundary is tracked in the whole space of parameters accounting for flow rate, surface tension, inclination and thermocapillarity. Especially, the latter two effects can strongly reduce the validity range of the Benney equation. It is also shown that the subcritical bifurcation found for falling films with the Benney equation is related to the blow-up of solutions and is unphysical in any case, even with the thermocapillary effect, in contrast with horizontally heated films. The accuracy of bounded solutions of the Benney equation is also analysed by comparison with a reference weighted integral boundary layer model. A distinction is made between closed and open flow conditions, when calculating travelling-wave solutions; the former corresponding to the conservation of mass and the latter to the conservation of flow rate. The open flow condition matches experimental conditions more closely and is explored for the first time through the associated dynamical system. It yields bounded solutions for larger Reynolds numbers than the closed flow condition. Finally, solutions that are conditionally bounded are found to be unstable to disturbances of larger periodicity. In this case, coalescence is the pathway yielding finite-time blow-up.

1. Introduction

Thin liquid film flows are widely present in various branches of industry. The length scale of the film flows may vary from some millimeters in cooling processes of electronic components to about ten meters in thin film evaporators in food and chemical industry. The liquid film is usually provided by a sprayer, being sub-cooled down to the saturation temperature for evaporation. In such a process, instabilities of free film surfaces play

† Chercheur qualifié, Fonds National de la Recherche Scientifique (Belgium)

a crucial role by inducing wavy regimes that are well known to enhance mass or heat transfer and may lead to film rupture (Colinet, Legros & Velarde 2001). From a fundamental point of view, thin film flows are a reference topic for the study of long-wave instabilities. The critical wavenumber at onset is zero implying that the waves are always long as compared to the film thickness. The cross-stream and streamwise scales are thus separated, similar to the separation of scales sustaining the boundary layer theory. The approximations that lead to the Prandtl (boundary layer) equations apply for film flows where the pressure is simply governed by gravity and surface tension (Chang 1994; Chang & Demekhin 2002).

1.1. *The film parameter*

In this context, it is a widespread practice to define a small parameter as the ratio of the film thickness and the typical length scale of disturbances of the flow. It is called *film parameter* and denoted by ε (Chang 1994). Contrary to usual situations and especially to the boundary-layer theory, the value of ε cannot be assigned a priori for film flows but is rather given a posteriori by the nonlinear solution itself. Indeed, the separation of scales is enabled by the smallness of the local steepness of the waves. It corresponds to small space and time modulations that reads

$$\partial_x, \partial_t \sim \varepsilon \ll 1. \tag{1.1}$$

At the linear stage, the film parameter can be associated to the neutral wavenumber k_c such that the maximum steepness of the waves is governed by the balance between the pressure drop due to surface tension and the pressure disturbance at the interface. For a vertical plane, it leads to the linear estimate $\varepsilon_L \sim k_c \propto (\mathrm{Re}/\mathrm{We})^{1/2}$, hence the common assumption $\mathrm{We}\,\varepsilon^2 \sim O(1)$ (Gjevik 1970) when $\mathrm{Re} = O(1)$; Re is the Reynolds number and We is the usual Weber number which compares the surface tension to the viscous stress at the interface as defined in (2.5). In the nonlinear regime, and at low Reynolds number where the flow is dominated by viscosity and surface tension, the maximum steepness of the wave is governed by a balance of the streamwise pressure gradient produced by surface tension and gravity along the plane. This leads to the nonlinear estimate $\varepsilon_N \sim \mathrm{We}^{-1/3}$.

In any case, at low Reynolds number, viscosity ensures the in-depth coherence of the flow which allows to reduce the full set of equations to a single evolution equation for the film thickness, as initially performed by Benney (1966). The equation is usually truncated at first or second order in ε and still referred to as the Benney equation (see the review by Oron *et al.* (1997)).

Now, the incompatibility between the two estimates ε_L and ε_N can be understood within the framework of the Benney expansion considering the assumption (1.1), where the genuine small parameter is $\varepsilon\mathrm{Re}$ instead of ε only. Thereby, the slaving of the velocity field to the film thickness evolution is ensured by the smallness of the product $\varepsilon\mathrm{Re}$. In the linear stage $\varepsilon_L\mathrm{Re} \sim (\mathrm{ReWe}^{-1/3})^{3/2}$, while in the nonlinear regime $\varepsilon_N\mathrm{Re} \sim \mathrm{ReWe}^{-1/3}$. Both estimates are then of the same order of magnitude and lead to the definition of a reduced Reynolds number $\mathcal{R} \propto \mathrm{ReWe}^{-1/3}$ as introduced by Shkadov (1977) and used later in this paper.

1.2. *Finite-time blow-up*

The Benney equation asymptotically predicts the linear stability threshold for the long-wave hydrodynamic instability in agreement with the Orr-Sommerfeld equation, which corresponds to the exact linear stability problem of the Navier-Stokes equations (Yih 1963). It also allows for bounded nonlinear *travelling-wave solutions*, *i.e.* waves that remain stationary in their moving frame, extending to *solitary waves*. Pumir *et al.* (1983)

have described such solitary waves as homoclinic trajectories of the associated dynamical system. They showed that there is a critical value Re_1^* above which these waves do not exist anymore. Besides, Pumir *et al.* (1983) completed their study by numerical simulations of the initial-value problem. They observed in simulations a catastrophic behaviour taking place for too large a Reynolds number ($\mathrm{Re} > \mathrm{Re}^*$) or too large an amplitude, showing a finite-time singularity (blow-up). They finally wrote that: "Re^* (above which catastrophic events occur) is obviously related to the critical value Re_1^* above which no one-hump solitary waves exist; however, we have not tried to check this numerically". Thanks to the recent numerical results by Oron & Gottlieb (2002), we will be able in this paper to "check this" for solitary waves as well as for any type of one-hump travelling waves (see §3).

The occurrence of finite-time blow-up observed with the Benney equation was never confirmed experimentally (Alekseenko *et al.* 1985; Liu & Gollub 1994). If the catastrophic behaviour encountered with the Benney equation were related to dry patch formation, it should be promoted by the thinness of the film – the thinner the film, the easier the formation of dry patch –, whereas the catastrophic behaviour is observed for thicker films ($\mathrm{Re} > \mathrm{Re}^*$). Again if this catastrophic behaviour were physical, it should also be observed with more elaborated models from which the Benney equation is derived (*e.g.* the boundary layer equations). Yet it has never been observed (Chang 1994).

Formally, the Benney equation is a particular case of the following evolution equation for the film thickness $h(x,t)$

$$\partial_t h + \partial_x \left(h^3 + \Phi\, h^m \partial_x h + h^3 \partial_{xxx} h \right) = 0, \tag{1.2}$$

where m is a positive integer and Φ a positive parameter. For $m = 6$, the Benney equation corresponding to a vertical and isothermal film (see §4.1) is recovered. Hocherman & Rosenau (1993) have conjectured that (1.2) leads to finite-time blow-up when $m > 3$. Bertozzi & Pugh (1998) refined this criterion proving that nonlinearities with exponents $m < 5$ can yield yet bounded solutions under certain conditions. Rosenau *et al.* (1992) have integrated equation (1.2) for $m = 6$ in time using a sinusoidal modulation of the film thickness as initial condition. They identified $\Phi^* \approx 0.5$ as limiting value separating uniformly bounded solutions and finite-time blow-up. This value appeared to be independent of the initial frequency of the disturbance.

All these previous works agree on identifying the strong nonlinearity $\partial_x(h^6\partial_x h)$, of inertial origin, as the cause of the singularities found with the Benney equation. Unfortunately, the addition of higher order terms reduces the range of validity even more (Salamon *et al.* 1994), asymptotical series having usually poor convergence properties. Hence the idea to regularize the asymptotic expansion as performed by Ooshida (1999) who formulated an evolution equation that does not lead to singularities for any value of the Reynolds number. However, his equation underestimates seriously the phase speed and the amplitude of waves at moderate Reynolds numbers. Therefore, far from threshold, it seems not possible to describe the flow dynamics by an unique evolution equation for the film thickness and other variables related to the velocity field should be introduced.

1.3. *Integral boundary layer approach*

Many authors since Kapitza & Kapitza (1949) and Shkadov (1967) have considered a model based on the Kármán-Polhausen averaging method and obtained by integrating the boundary layer equations across the film thickness. It results into two coupled equations for the film thickness $h(x,t)$ and the local flow rate $q(x,t)$. This model, referred to as the Shkadov model, allows for a better description of the flow dynamics for much larger Reynolds numbers and does not suffer any singularity. However, contrary to the

Benney equation the model derived by Shkadov (1967) does not predict the correct threshold of the long-wave instability. Recently, Ruyer-Quil & Manneville (2000, 2002) have cured this discrepancy by combining a systematic gradient expansion with weighted residual techniques using polynomials as test functions. Applying a Galerkin method, they obtained a model involving also the two fields h and q. The linear stability analysis of this model remarkably agrees with the Orr-Sommerfeld results, at least up to moderate Reynolds numbers (Re $\sim$ 50). In the strongly nonlinear regime, the spatial evolution of the solutions to this model in the presence of noise or periodic forcing compares quantitatively to both experiments (Liu & Gollub 1994) and direct numerical simulations (Ramaswamy *et al.* 1996).

Yet, the Benney equation models in the simplest way the dynamics of film flows. It even faithfully captures all physical mechanisms at small Reynolds numbers and its widespread use still confirms its interest (Oron *et al.* 1997). For this reason, the knowledge of its validity in the parameter space – *i.e.* where solutions exist or not and if yes, how accurate they are – is crucial. This paper is mainly dedicated to this issue and the weighted integral boundary layer model of Ruyer-Quil & Manneville will constitute our model of reference.

1.4. *Benney equation with Marangoni effect*

When a temperature gradient is applied across a horizontal fluid layer, the layer being heated from below, two mechanisms related to the Marangoni (thermocapillary) effect can lead the liquid layer from a quiescent conducting state to convective motions (Colinet *et al.* 2001). Both of them originate from the interfacial stress generated at the interface by the surface tension gradient. This gradient can have two origins, a modification of the temperature distribution in the bulk due to the advection by the velocity field, or a modulation of the free surface elevation, both of them generating a temperature gradient at the interface. The two mechanisms were classified by Goussis & Kelly (1991) as the P-mode and the S-mode, respectively. The P-mode generally yields convection rolls or hexagonal or square cells, the size of which is of the same order of magnitude than the depth of the layer. This instability is referred to as the *Marangoni–Bénard instability* and was theoretically evidenced by Pearson (1958). This instability does not request a deformable free surface. The S-mode produces large-scale deformations, the horizontal size of which is much larger than the depth of the layer, and may generally lead to film rupture. This instability is referred to as the *long-wave Marangoni instability* and was first theoretically evidenced by Scriven & Sterling (1964), who neglected the gravity, which was later corrected by Smith (1966). Since this work is exclusively devoted to the problem of long-wave deformations, speaking about the Marangoni effect will always refer to the thermocapillary long-wave instability, or S-mode, while the P-mode will be merely disregarded.

As said above, the long-wave thermocapillary instability leads to film rupture for horizontal layers (Krishnamoorthy & Ramaswamy 1995). Boos & Thess (1999) followed numerically the evolution of a film profile towards rupture using the Navier-Stokes equation in combination with a linear temperature field, and identified a cascade of consecutive 'structuring events'. The qualitative agreement between their results and those obtained from the long-wave approximation for horizontal layers (Oron 2000) indicates that the main features of the physical system are well captured by this approximation. Weakly nonlinear analysis done by VanHook *et al.* (1997) has demonstrated the subcritical character of the pure long-wave Marangoni instability, *i.e.* for a horizontal film. Thiele & Knobloch (2004) studied the transition between a horizontal and a slightly inclined layer in the presence of the Marangoni effect. They showed that the bifurcation analysis for

the horizontal case shares its properties with the inclined problem only for very small values of the inclination angle. For larger inclinations the system behaves much more like a "falling film" even though their theory does not retain inertial effects and the dominant balance in the direction normal to the wall is still hydrostatic. As a consequence, Thiele & Knobloch (2004) found the bifurcation (from the flat film state) to be always subcritical for very small inclinations, and always supercritical for sufficiently large inclinations.

For inclined and vertical walls, the Marangoni effect has been incorporated into the Benney equation by (Joo *et al.* 1991). They examined numerically the interaction of the two instability modes, namely hydrodynamic and thermocapillary (S-mode) instabilities. They found that thermocapillarity enhances the hydrodynamic instability and promotes the dramatic behaviour already encountered for isothermal films. They associated this behaviour with the limitation of weakly nonlinear results obtained by Gjevik (1970) and Lin (1974) where none of the solutions are stable for small wavenumbers. However, weakly nonlinear analysis involves only a small number of harmonics and cannot represent the highly nonlinear waves observed by Kapitza & Kapitza (1949) or computed by Pumir *et al.* (1983). In the present work, the 'dramatic behaviour' found by Joo *et al.* (1991) will be rather linked to the finite-time blow-up of the Benney equation whose the nature will appear to be totally different to the one leading to film rupture for horizontal layers (Krishnamoorthy & Ramaswamy 1995).

1.5. *Frame and objectives of this work*

The objective of this paper is to study the blow-up behaviour of the Benney equation and its dependence on the Reynolds number, the Kapitza number, the inclination angle and the Marangoni number. These numbers measure, respectively, the flow rate, the surface tension, the hydrostatic pressure and the thermocapillarity. The emphasis will be put on the dependence of the existence of the wave solutions on their wavenumber.

To study the solution behaviour we employ bifurcation analysis using numerical continuation techniques (Doedel *et al.* 1997). Continuation is an effective method to determine branches of stationary solutions and their bifurcations by following them through the parameter space (Doedel *et al.* 1991*a*,*b*). For thin films, continuation was applied in studies of travelling and solitary waves of film flows down inclined walls (Chang 1994; Ruyer-Quil & Manneville 2000, 2002; Scheid *et al.* 2002), sliding drops on slightly inclined planes (Thiele *et al.* 2001, 2002) or base states of locally heated falling films (Skotheim *et al.* 2002).

To compute travelling-wave solutions an additional constraint is required that specifies the 'flow condition' in their moving frame. It is related to the choice of the conserved quantity. The 'closed flow' condition corresponds to the conservation of the fluid mass and the 'open flow' condition, to the conservation of the flow rate. Chang (1994) already evocated this condition speaking about constant-average thickness or constant-flux formulation. Many authors, as for instance (Joo *et al.* 1991; Salamon *et al.* 1994; Oron & Gottlieb 2002; Scheid *et al.* 2002), implicitly prescribed the closed flow condition. This is due to the fact that in time-dependent simulations, using periodic boundary conditions, the amount of liquid leaving the domain downstream is reinjected upstream. However, the open flow condition is more appropriate to the experimental situation of a flow on an inclined plate when a periodic forcing is imposed at the inlet (Kapitza & Kapitza 1949; Liu *et al.* 1993; Liu & Gollub 1994). Indeed, Ruyer-Quil & Manneville (2000) found satisfactory agreement with the phase speeds of two-dimensional travelling-wave solutions from Kapitza's experiments using the open flow condition, whereas the closed flow condition resulted in deviations of up to 15%.

We restrain the present study to the two-dimensional case for at least the three follow-

ing reasons: (i) we want to benefit from the dynamical-system theory (see §2.1.2) that cannot be applied with a third coordinate; (ii) the linear growth rate of transverse waves was found by Goussis & Kelly (1991) to be always larger than that of longitudinal rolls as far as the long-wave modes are concerned. Note that this result extends the one obtained for the pure hydrodynamic mode by Yih (1955) who extended the Squire's approach to free surface flows (Huerre & Rossi 1998); (iii) as a consequence of the previous point and as shown experimentally, it always exists a transition zone of purely two-dimensional flow when the film is periodically forced at the inlet (Liu *et al.* 1995). Moreover, the secondary three-dimensional instability develops at a certain distance from the inlet that increases with decreasing Reynolds numbers (Alekseenko *et al.* 1994). Since the Benney equation applies for small Reynolds numbers only, we thus expect a large zone where two-dimensional waves are dominant. Obviously, the situation will be different in presence of transverse perturbations of finite-amplitude, especially in the case of a heated falling film when the thermocapillary effect will promote the formation of rivulets (Joo *et al.* 1996; Ramaswamy *et al.* 1997). However, this is beyond the scope of the present work.

In §2 the mathematical formulation including the Marangoni effect is presented for both the Benney equation and our reference model. The closed and open flow conditions are also detailed. In §3 we compare travelling-wave solutions of the Benney equation with those of the reference model. Then, we obtain the boundary beyond which the Benney equation does not possess any stationary solution by scanning the Reynolds number in the whole spectrum of unstable wavenumbers, *i.e.* from neutrally unstable modes to infinite wavelength solitary waves. This boundary will be called *absence-of-solution boundary* and will be linked to the *blow-up boundary* found with time-dependent simulations by Oron & Gottlieb (2002). In §4 we track the absence-of-solution boundary through the parameter space, investigating successively the influence of surface tension, inclination and thermocapillarity. Below this boundary, the accuracy of the solutions of the Benney equation is determined. The influence of Marangoni effect on the subcritical behaviour is also addressed. Finally, §5 is devoted to the stability of the stationary solutions of the Benney equation in the region where the blow-up occurs at a finite wavenumber. A Floquet analysis is used to show their instability to disturbances of large period implying the possibility of finite-time blow-up via wave coalescence. Section 6 presents the concluding remarks.

2. Evolution equations and methodology

We consider a liquid film flowing down a heated wall of constant temperature $T_{\rm w}$, of inclination to the horizontal β, and bounded by a passive gas of temperature T_∞ (see figure 1). The liquid is Newtonian and of constant density ρ, kinematic viscosity ν and thermal conductivity κ. The surface tension is assumed to decrease linearly with increasing temperature, $\sigma = \sigma_\infty - \gamma(T - T_\infty)$, where σ_∞ is the surface tension at the gas temperature and γ is positive. The heat transfer coefficient from the liquid to the gas is denoted by α. The length and time scales are defined without reference to the flow characteristics as

$$l_\nu = \left(\frac{\nu^2}{g}\right)^{1/3} \quad \text{and} \quad t_\nu = \left(\frac{\nu}{g^2}\right)^{1/3},$$

respectively, where g is the gravitational acceleration. We use a coordinate system (x, y) with the origin at the wall, x directed streamwise and y normal to the wall increasing into the liquid. The coordinates are scaled by l_ν. The liquid properties, the temperature

difference $\Delta T = T_\mathrm{w} - T_\infty$ and the inclination angle determine the dimensionless numbers

$$\mathrm{Ka} = \frac{\sigma_\infty\, l_\nu}{\rho\,\nu^2}, \quad \mathrm{Ma} = \frac{\gamma\,\Delta T l_\nu}{\rho\,\nu^2}, \quad \mathrm{Bi} = \frac{\alpha\, l_\nu}{\kappa}, \quad \text{and} \quad \mathrm{S} = \sin\beta. \tag{2.1}$$

The Kapitza (resp. Marangoni) number compares surface tension (resp. thermocapillarity) to viscosity and gravity. The Biot number describes the rate of heat transport from the liquid to the ambient gas. The number S obviously measures the wall inclination.

2.1. *The Benney equation*

Because the typical wavelength λ of waves at the free surface is much larger than the film thickness, long-wave asymptotics as proposed by Benney (1966) is used to describe the evolution of the flow. The full system of governing equations and boundary conditions can be reduced to a single evolution equation for the local position of the free surface $y = h(x,t)$:

$$\partial_t h + \partial_x \left(\mathrm{S}\frac{h^3}{3} + \frac{2}{15}\mathrm{S}^2 h^6 \partial_x h - \sqrt{1-\mathrm{S}^2}\,\frac{h^3}{3}\partial_x h + \mathrm{Ka}\frac{h^3}{3}\partial_{xxx} h + \frac{h^2}{2}\frac{\mathrm{Bi}\,\mathrm{Ma}\,\partial_x h}{(1+\mathrm{Bi}\,h)^2} \right) = 0. \tag{2.2}$$

The first term inside the parenthesis accounts for the driving force due to gravity, the second one originates from inertia and causes the hydrodynamic (surface-wave) instability, the third and fourth ones represent the stabilizing effects of the hydrostatic pressure and the surface tension, respectively, and the last one is responsible for the thermocapillary instability. Equation (2.2) was obtained by Joo *et al.* (1991). However, here we neglect evaporation that was included there. Though (2.2) with $\mathrm{Ma} = 0$ is usually called the Benney equation (BE), we will also use this generic name for equation (2.2) with the Marangoni effect. Remark finally, that (2.2) is $\varepsilon-$free contrary to the equation obtained by Joo *et al.* (1991). The reason is that the we have used the same length scale l_ν for both directions x and y together with the long-wave assumption (1.1) (see also discussion of equation 2.13).

In experiments, the control parameter that determines the Nusselt film thickness $\bar{h}_\mathrm{N}$ is the specific volumetric flow rate $\bar{q}_\mathrm{N}$ (Kapitza & Kapitza 1949; Liu *et al.* 1993; Kabov *et al.* 2002). We denote its dimensionless form by $q_\mathrm{N} = \bar{q}_\mathrm{N}/\nu$. The Reynolds number is commonly defined as

$$\mathrm{Re} = q_\mathrm{N}. \tag{2.3}$$

Nusselt (1916) determined the flat film solution that has the dimensionless thickness

$$h_\mathrm{N} = \frac{\bar{h}_\mathrm{N}}{l_\nu} = \left(\frac{3\mathrm{Re}}{\mathrm{S}}\right)^{1/3}. \tag{2.4}$$

Let us also define the Weber number

$$\mathrm{We} = \frac{\sigma_\infty}{\rho g \bar{h}_\mathrm{N}^2 \sin\beta} = \frac{\mathrm{Ka}}{\mathrm{S}h_\mathrm{N}^2} \tag{2.5}$$

that we will need in the following to compare our results with literature.

2.1.1. *Linear stability*

To analyse the linear stability of the uniform flat film one imposes a small harmonic disturbance by writing

$$h = h_\mathrm{N} + a\exp\left\{\mathrm{i}\,(k\,x - c\,t) + \Gamma\,t)\right\}, \tag{2.6}$$

where a, k, c and Γ are, respectively, the real amplitude, wavenumber, phase speed and growth rate of the disturbance. Inserting the normal-mode representation (2.6) into (2.2) and linearizing in a yield the linear phase speed and growth rate:

$$c_{\text{L}} = \text{S}h_{\text{N}}^2, \tag{2.7}$$

$$\Gamma = k^2 h_{\text{N}}^3 \left(\frac{2}{15}\text{S}^2 h_{\text{N}}^3 - \frac{1}{3}\sqrt{1-\text{S}^2} + \frac{1}{2}\frac{\text{Bi}\,\text{Ma}}{h_{\text{N}}(1+\text{Bi}\,h_{\text{N}})^2} - \frac{1}{3}\text{Ka}\,k^2 \right). \tag{2.8}$$

The surface waves will grow for $\Gamma > 0$, *i.e.* for disturbance wavenumbers smaller than the neutral (cut-off) wavenumber

$$k_{\text{c}} = \frac{1}{\text{Ka}^{1/2}} \left(\frac{2}{5}\text{S}^2 h_{\text{N}}^3 - \sqrt{1-\text{S}^2} + \frac{3}{2}\frac{\text{Bi}\,\text{Ma}}{h_{\text{N}}(1+\text{Bi}\,h_{\text{N}})^2} \right)^{1/2}, \tag{2.9}$$

or larger than $k_{\text{c}} = 0$, which justifies the long-wave approximation. This primary instability corresponds to a *Hopf bifurcation* from the flat film solution. The emerging branch of solutions will be *supercritical* (resp. *subcritical*) if it bifurcates towards the region where $k < k_{\text{c}}$ (resp. $k > k_{\text{c}}$). The *neutral curve* is the locus where the monochromatic linear modes (waves) are of wavenumber k_{c}.

2.1.2. *Travelling-wave solutions*

We seek travelling-wave solutions, *i.e.* stationary solutions of Eq. (2.2) in a frame of reference moving downstream at speed c. Introducing $h(x,t) = h(\xi)$ with $\xi = x - c\,t$, (2.2) can be integrated once to yield

$$-c\,h + \text{S}\frac{h^3}{3} - Q + \frac{2}{15}\text{S}^2 h^6 h' + \text{Ka}\frac{h^3}{3}h''' - \sqrt{1-\text{S}^2}\,\frac{h^3}{3}h' + \frac{h^2}{2}\frac{\text{Bi}\,\text{Ma}\,h'}{(1+\text{Bi}\,h)^2} = 0, \tag{2.10}$$

where the prime denotes the derivative with respect to ξ. Q is the integration constant and represents the flow rate in the moving frame of reference, as shown in the following by (2.15). Its value is negative because the phase speed c of surface waves is generally larger than the mean velocity of the film (three times at criticality). Assuming that no dry spots are possible ($h \neq 0$), (2.10) can be divided by $-\text{Ka}\,h^3/3$ to get

$$h''' = F[h,h'] = \frac{1}{\text{Ka}}\left(\frac{3}{h^3}(Q + c\,h) - \text{S} - \frac{2}{5}\text{S}^2 h^3 h' + \sqrt{1-\text{S}^2}\,h' - \frac{3}{2}\frac{\text{Bi}\,\text{Ma}\,h'}{h(1+\text{Bi}\,h)^2} \right). \tag{2.11}$$

The differential equation (2.11) is recast into a dynamical system, *i.e.* a system of first order differential equations, as follows

$$\left\{ \begin{array}{ll} U_1' = & U_2 \\ U_2' = & U_3 \\ U_3' = & F[U_1, U_2] \end{array} \right. \tag{2.12}$$

where $U_1 = h$, $U_2 = h'$ and $U_3 = h''$.

To determine iteratively the periodic solutions of the dynamical system (2.12), we use the continuation and bifurcation tools for ordinary differential equations AUTO 97 (Doedel *et al.* 1997). During computations the periodicity of the solution is enforced, the phase is fixed by $U_1|_{\xi=0} = h_{\text{N}}$ and the total volume $\int_0^1 U_1\,d\xi = \langle h \rangle_\xi$ is controlled as specified in §2.3. This amounts to one integral and four boundary conditions, hence the continuation requires three free parameters (Keller 1977). Fixing the set of parameters $\{\text{Ka}, \text{Ma}, \text{Bi}, \text{S}, h_{\text{N}}\}$ the free parameters are $\{k, c, Q\}$. The continuation is started from the neutral mode corresponding to the Hopf bifurcation point with k_{c} and c_{L}. The starting

value of Q is fixed by the Nusselt solution $h(\xi) = h_{\rm N}$ such that from (2.10) $Q_{\rm L} = {\rm S}h_{\rm N}^3/3 - h_{\rm N}\, c_{\rm L}$.

As announced in §1, the estimate of the aspect ratio $\varepsilon_L = h_{\rm N}/\lambda$ is obtained a posteriori through the wavenumber $k = 2\pi/\lambda$ of the stationary wave solution, and reads

$$\varepsilon_L = \frac{h_{\rm N} k}{2\pi}. \tag{2.13}$$

In contrast with several previous works (Joo *et al.* 1991, 1996; Scheid *et al.* 2002), the value of the aspect ratio is not assumed a priori. However, doing so results merely in a rescaling of λ, as for instance in Joo *et al.* (1991) where the wavenumber is defined by $k_{\rm JDB} = h_{\rm N} k/\varepsilon_{\rm JDB}$ with fixed $\varepsilon_{\rm JDB} = 0.2$. It results merely that $k_{\rm JDB}$ remains of $O(1)$.

2.2. *The weighted integral boundary layer model (WIBL)*

Ruyer-Quil & Manneville (2000) elaborated a model that predicts accurately and economically the linear and nonlinear properties of film flows up to relatively high Reynolds numbers. This model was derived in the frame of the integral boundary layer (IBL) approximation by combining a gradient expansion to weighted residual techniques with polynomials as test functions. The corresponding first-order weighted integral boundary layer (WIBL) model including the Marangoni effect is derived in appendix §A and reads

$$\partial_t h = -\partial_x q, \tag{2.14a}$$

$$\partial_t q = \frac{5}{6}{\rm S}h - \frac{5}{2}\frac{q}{h^2} + \frac{9}{7}\frac{q^2}{h^2}\partial_x h - \frac{17}{7}\frac{q}{h}\partial_x q - \frac{5}{6}\sqrt{1-{\rm S}^2}h\,\partial_x h + \frac{5}{6}{\rm Ka}\,h\,\partial_{xxx} h + \frac{5}{4}\frac{{\rm Ma\,Bi}\,\partial_x h}{(1+{\rm Bi}\,h)^2}, \tag{2.14b}$$

where q is the local flow rate. Equation (2.14a) is the mass conservation equation. The terms on the right-hand side of (2.14b) account, from the left to the right, for gravity, viscous dissipation, inertia (two terms), hydrostatic effect, surface tension and thermocapillary effect. The above model does not experience any singularity and will be used as reference model in the following to describe the travelling-wave regime. Notice that the long-wave expansion of (2.14) (see appendix A) leads directly to the BE (2.2) so that the physics included in the BE is already present in the WIBL model.

In a moving frame of reference $\xi = x - c\,t$, (2.14a) can be integrated to yield

$$q = c\,h + Q. \tag{2.15}$$

and assuming as before $h \neq 0$, (2.14b) gives

$$h''' = F_{\rm WIBL}[h, h'] = \frac{1}{\rm Ka}\left(\frac{3}{h^3}(Q + c\,h) - {\rm S} - \frac{54}{35}\frac{Q^2 h'}{h^2} + \frac{6}{35}\frac{c\,h'}{h^2}(c\,h - Q) + \sqrt{1-{\rm S}^2}h' - \frac{3}{2}\frac{{\rm Bi\,Ma}\,h'}{h(1+{\rm Bi}\,h)^2}\right). \tag{2.16}$$

The value of the integration constant Q represents, as in §2.1.2, the (negative) mean flow rate in the moving frame of reference, *i.e.* underneath the wave. The periodic stationary solutions of (2.16) are determined using the dynamical system (2.12) by simply replacing F by $F_{\rm WIBL}$. Notice that (2.11) and (2.16) differ only by the inertial terms.

2.3. *Closed and open flow conditions*

Periodic boundary conditions, commonly implemented in numerical simulations, correspond to a closed flow, for which the liquid flowing out is reinjected at the inlet. Therefore

the *closed flow condition* reads

$$X\big|_{x=\lambda} = X\big|_{x=0} \quad \forall t \tag{2.17}$$

where X refers to any flow variable and λ is the length of the domain. Nevertheless, because the flow is gravity-oriented, the closed flow condition cannot be achieved experimentally. Indeed in experiments, the flow is open and when, at the inlet, the film is furthermore forced at a given frequency, the waves keep their periodicity in time, at least before the onset of secondary instabilities. In this situation, the *open flow condition* can be written as

$$X\big|_{t=\tau} = X\big|_{t=0} \quad \forall x \tag{2.18}$$

where τ is the period.

We shall discuss those conditions using the mass conservation equation (2.14a). In the case of a periodic modulation of the film surface, the space average of $\partial_t h + \partial_x q = 0$, together with the closed flow condition (2.17), gives

$$\frac{\mathrm{d}}{\mathrm{d}t}\langle h\rangle_x = 0 \tag{2.19}$$

where $\langle\cdot\rangle_x = \frac{1}{\lambda}\int_0^\lambda \cdot\, dx$. The amount of liquid in the domain is constant at any time t and equal to its value at initial time. Transposing this condition to the computation of travelling waves yields

$$\langle h\rangle_\xi = h_\mathrm{N}, \tag{2.20}$$

which will be referred hereafter to as the *closed flow condition*.

Turning to a time periodic modulation of the film surface, the time average of (2.14a), together with the open flow condition (2.18), gives

$$\frac{\mathrm{d}}{\mathrm{d}x}\langle q\rangle_t = 0. \tag{2.21}$$

The average flow rate is independent of the location x and therefore equal to its inlet value. Again transposing this condition to the computation of travelling waves reads

$$\langle q\rangle_\xi = q_\mathrm{N}, \tag{2.22}$$

which will be referred hereafter to as the *open flow condition*.

The consequence in the choice of the flow condition for travelling-wave solutions appears now by averaging (2.15):

$$\langle h\rangle_\xi = \frac{\langle q\rangle_\xi - Q}{c}. \tag{2.23}$$

In experiments, for which the open flow condition applies, the control parameter is the flow rate at the inlet whose dimensionless value is the Reynolds number $\mathrm{Re} = q_\mathrm{N}$. Then (2.22) with (2.23) shows that the average film thickness $\langle h\rangle_\xi = (\mathrm{Re} - Q)/c$ will be influenced by the wave features c and Q. For instance, Alekseenko *et al.* (1994) have observed experimentally a decrease of the average film thickness downstream related to an increase of the phase speed of travelling waves. On the contrary, if we impose the closed flow condition, the insertion of (2.20) into (2.23) gives $\langle q\rangle_\xi = ch_\mathrm{N} + Q$. This implies that the effective flow rate $\langle q\rangle_\xi$ will deviate from the imposed one $q_\mathrm{N} = \mathrm{S}h_\mathrm{N}^3/3$ (*i.e.* Re) depending on the evolution of the travelling waves. For instance, an increase of the phase speed leads to an underestimation of the Reynolds number $q_\mathrm{N} < \langle q\rangle_\xi$.

3. Blow-up of the Benney equation for closed flows

Salamon *et al.* (1994) computed travelling-wave solutions of the Navier-Stokes equations for a film falling on a vertical (S = 1) and isothermal (Ma = 0) wall varying Re at fixed We = 1000 and $\varepsilon_L = 0.04/2\pi$. They imposed the closed flow condition (2.20). The solid line in figure 2 shows their results for the reduced maximum film thickness $h_{\max}/h_{\rm N}$ of the solutions †. Using the dynamical system (2.12) with (2.16), we computed the curve corresponding to the WIBL model (dot-dashed line). Note the remarkable agreement with the Salamon *et al.*'s results in this range of Reynolds numbers. On the contrary, the curve computed for the BE with (2.11) (dashed line) shows a fold at $\mathrm{Re}^* \simeq 4.8$. Oron & Gottlieb (2002) computed corresponding travelling-wave solutions performing time-dependent simulations of the BE (circles). They only found stable solutions for the small amplitude part of the dashed curve. Those solutions are *bounded* and exist only for $\mathrm{Re} < \mathrm{Re}^*$. For $\mathrm{Re} > \mathrm{Re}^*$, the BE exhibits no stationary wave solution and any perturbation of the flat film is *unbounded*, *i.e.* it yields *finite-time blow-up*: $h(x^*, t) \to \infty$ at some point x^* as $t \to t^* < \infty$.

Now, let us calculate families of stationary solutions of the BE and the WIBL model and characterize the blow-up of the BE in the whole spectrum of unstable wavenumbers.

3.1. *Families of stationary solutions*

For a vertically falling and isothermal film, Chang *et al.* (1993) constructed the travelling-wave solutions bifurcating from the neutral stability curve as a function of their wavenumber for the boundary-layer equation (see appendix A) at moderate Reynolds number. They distinguished two main families of waves. The first one referred to as *hole wave family* and denoted by γ_1 terminates at small wavenumbers by slow solitary-like waves with a dominant depression, *i.e.* $h_{\max} - h_{\rm N} < h_{\rm N} - h_{\min}$. The second family referred to as *hump wave family* and denoted by γ_2 corresponds to fast waves with a dominant elevation. The γ_1 and γ_2 families can bifurcate either in respective Hopf and period doubling bifurcations, or vice versa. Actually, the bifurcations of the families may be reversed if the dispersion of the waves is modified (Salamon *et al.* 1994). The Kawahara equation that contains such dispersion terms has been studied by Chang *et al.* (1993). They showed that the existence of the two families of slow and fast waves bifurcate in an imperfect pitchfork bifurcation (Drazin 1992) from a family of standing waves (that travel at exactly three times the average velocity of the flow). Such a bifurcation is sensitive to the dispersive effects as shown below.

The bifurcation diagram in figure 3 shows as solid lines the two first wave families of the BE characterized by the reduced maximum wave thickness $g = h_{\max}/h_{\rm N}$ and the phase speed $c/c_{\rm L}$ (where $c_{\rm L}$ is the linear phase speed) as a function of the wavenumber k. The parameters are Re = 2.0667, Ka = 3375, S = 1 and Ma = 0, which correspond to a vertically falling, isothermal film of water at 20°C (see ‡ and table 1). The closed flow condition is enforced. The γ_2 family starts at cut-off wavenumber $k_{\rm c}$ corresponding to the Hopf bifurcation point (HB). This bifurcation is *supercritical*, so the wavelength of solutions is larger than at threshold $2\pi/k_{\rm c}$. It yields stationary waves that become increas-

† Note that the parameters We and ε_L depend both on $h_{\rm N}$ (see 2.5 and 2.13); remember that $h_{\rm N} = (3\mathrm{Re}/\mathrm{S})^{1/3}$. Hence the fluid properties change continuously along the curves in figure 2 since for increasing Re, Ka increases proportionally to $\mathrm{Re}^{2/3}$ and the wavenumber k of the travelling-wave solutions decreases proportionally to $\mathrm{Re}^{-1/3}$. This drawback is cured with our scaling where Re accounts alone for the dimensionless Nusselt film thickness.

‡ Some authors we refer to (Salamon *et al.* 1994; Oron & Gottlieb 2002) based the Reynolds number on the surface velocity rather than on the mean velocity, which yields R = 3Re/2. Therefore, Re = 2.0667 corresponds to R = 3.1 and Ka = 3375 to We = 1000 with $h_{\rm N} = 1.8371$.

ingly one-hump and faster as k decreases. In the limit $k \to 0$, the solutions correspond to homoclinic orbits in the phase space and will be referred to as *homoclines*. The γ_2 family appears by period doubling (PD). The corresponding waves become increasingly one-hole and slower as k decreases.

As the wavenumber decreases, higher harmonics become linearly unstable at $k_n = k_c/n$ with $n = 2, 3, \ldots$. The resulting families $\gamma_{1,2}^n$ for $n > 1$ correspond therefore to n-hump or n-hole travelling-wave solutions. Their maximum heights $g^n(k)$ are not displayed in figure 3 because they are *homothetic* in k, *i.e.* given that $g^n(k_n) = g(k_c)$ it follows that $g^n(k/n) = g(k)$. The individual solutions correspond simply to n identical solutions of the $n = 1$ family placed in a domain of size $2\pi n/k$.

The dashed lines in figure 3 represent the wave families computed with the WIBL model. In contrast with the BE, the γ_2 family appears by period doubling while the γ_1 family emerges from the cut-off wavenumber. As already mentioned, this disagreement can be understood considering the sensitivity of the imperfect pitchfork bifurcation to slightly different dispersions which originate from the different accounts for the inertial effects (compare 2.11 with 2.16). The intersection point (IP) between γ_1 and γ_2 families for the WIBL model indicates the wavenumber below which hole and hump wave solutions are discernible.

On figure 3, the differences between the maximal amplitudes of hump solutions computed with the BE and the WIBL model do not exceed 10% and are even much smaller for hole solutions. The comparison of profiles of one-hump travelling-wave solutions is displayed in figure 4. The corresponding wavenumbers are pointed by arrows at the top of figure 3. We can conclude that for the given parameters, the agreement of BE and WIBL model is satisfactory in the whole spectrum of wavenumbers.

Because the hump solutions have a larger maximal film thickness $h_{\max}$ than the hole ones, they will be subject to blow up at smaller Reynolds number. This can be understood from the nature of the strongly nonlinear term $\sim \partial_x(h^6\partial_x h)$ in (2.2) responsible for singularities. Similarly, at a given k the one-hump solutions are more "dangerous" than multi-hump ones. Indeed, Pumir *et al.* (1983) observed that during evolution the only kind of wave that could be recognized is the one-hump solution. It evolves into a solitary wave and then blows up in finite-time for $\mathrm{Re} > \mathrm{Re}^*$. Hence, we will only focus in the following on one-hump travelling-wave solutions in order to discuss the validity domain of the BE, first in terms of their existence and next in terms of their accuracy. Their stability will be addressed later in §5.

3.2. *Blow-up versus wavenumber*

In this section, we analyse the existence of one-hump wave solutions of the BE and show that the occurrence of their absence is closely linked to the finite-time blow-up observed in simulations.

The bifurcation diagram in figure 5 shows in solid lines families of one-hump travelling-wave solutions computed with the BE for several Re. The fixed parameters $\mathrm{S} = 1$, $\mathrm{Ma} = 0$ and $\mathrm{Ka} = 2950$ correspond to a vertically falling, isothermal film of water at $15°C$ (see table 1) like in experiments by Kapitza & Kapitza (1949). The closed flow condition (2.20) has been used. The dashed curves are the corresponding wave families computed with the WIBL model. For $\mathrm{Re} \gtrsim 3$, the BE wave families feature a *saddle-node* bifurcation at k^* indicated by an asterisk. This implies that for $k < k^*$ the BE has no stationary solution of γ_2 fast wave type. For $k > k^*$, two stationary solution branches coexist. Pumir *et al.* (1983) and Oron & Gottlieb (2002) have shown that only the lower branch of small amplitude solution corresponds to bounded solutions (note that the WIBL model does not possess the larger amplitude branch at all). The bifurcation at k_c is supercritical

for $\mathrm{Re} \leq 5$. However, the interval $[k^*, k_c]$ shrinks with increasing Re until vanishing. For larger Re the Hopf bifurcation becomes subcritical. Note the intrinsic structure of the families for $\mathrm{Re} = 5.75$ and 6 where a second saddle-node is present as indicated by a cross on figure 5.

In figure 6 we plot the locus denoted by k^* of the saddle-node bifurcations of the γ_2 family as a function of Re (dashed line), together with the cut-off wavenumber k_c (solid line). The flat film is linearly stable above k_c, one-hump γ_2 travelling-wave solutions can be found between the solid and the dashed line only. The asterisks and crosses indicate the saddle-node bifurcation points obtained in figure 5. The inset of figure 6 shows the existence of a sub-domain bounded from below by the solid curves and by the dashed lines otherwise. The solutions in this domain are always unstable since they originate from a subcritical bifurcation (see for instance $\mathrm{Re} = 6$ wave family in figure 5). This subcritical behaviour is most likely non-physical and has at least not been observed with our reference model. This behaviour will be analysed in more details in §4.4.2.

Oron & Gottlieb (2002) have performed simulations of travelling-wave solutions for various wavenumbers k and obtained a boundary for finite-time blow-up as marked out by circles in figure 6. This boundary match perfectly the absence-of-solution one for one-hump travelling waves, except the two points at the bottom. Those latter rather match the absence-of-solution boundary of two-hump solutions, *i.e.* for $n = 2$ (dotted line in figure 6). The sensibility to initial conditions in simulations could explain this discrepancy. Anyway, our results show unequivocally, and for the whole spectrum of unstable wavenumbers, the link between the saddle-node bifurcation point of the BE for γ_2 wave family and the finite-time blow-up observed in simulations.

We are now able to define two particular values of the Reynolds number as indicated in figure 6: Re_h^* for $k^* \to 0$ at which only homoclines become singular and Re_c^* for $k^* = k_c$ at which all the linearly unstable modes lead to singularities. Re_h^* and Re_c^* will be used to globally feature the validity domain of the BE. For the sake of clarity, and since we have identified the finite-time blow-up boundary to the absence-of-solution one, we will only refer to the former in what follows.

4. Parametric study for closed and open flows

In this section, we first study systematically the blow-up features of the BE for falling films on vertical and isothermal walls. Thereby, both closed and open flow conditions are analysed. The accuracy of the stationary solutions of the BE (when they exist) is determined using again the WIBL model as reference. Finally, the influences of inclination and Marangoni effect are investigated.

4.1. *Reduced systems and parameters*

Keeping track of the domain boundaries in parameter space where stationary solutions exist is quite involved. Indeed, five parameters can be varied, namely the inclination of the plane (S), surface tension (Ka), its sensitivity to temperature (Ma), the heat transfer at the interface (Bi) and finally the inlet flow rate (Re). Fortunately, at first order – due to the neglect of viscous streamwise dissipation – the number of parameter can be reduced by one applying a transformation proposed initially by Shkadov (1977). This number can even be reduced to three in the reasonable limit of small Biot number (see appendix B and table 1).

Shkadov's transformation can be written as: $x \to \mathcal{L}\, x$, $h \to h_N\, h$, $t \to \mathcal{L}\, t/(\mathrm{S} h_N^2)$, where

$\mathcal{L} = (\mathrm{Ka}\, h_\mathrm{N}/\mathrm{S})^{1/3}$ with $h_\mathrm{N} = (3\mathrm{Re}/\mathrm{S})^{1/3}$. The BE (2.2) then becomes

$$\partial_t h + \partial_x \left(\frac{h^3}{3} + \frac{2}{15}\mathcal{R}\, h^6\, \partial_x h - \mathcal{C}\frac{h^3}{3}\partial_x h + \frac{h^3}{3}\partial_{xxx} h + \frac{h^2}{2}\frac{\mathcal{M}\,\mathcal{B}\,\partial_x h}{(1+\mathcal{B}\,h)^2} \right) = 0, \qquad (4.1)$$

where

$$\mathcal{R} = \mathrm{S}\frac{h_\mathrm{N}^4}{\mathcal{L}}, \qquad \mathcal{C} = \cot\beta \frac{h_\mathrm{N}}{\mathcal{L}}, \qquad \mathcal{M} = \frac{\mathrm{Ma}}{\mathrm{S}h_\mathrm{N}\mathcal{L}} \quad \text{and} \quad \mathcal{B} = h_\mathrm{N}\mathrm{Bi}.$$

Similarly the WIBL model (2.14) with $q \to \mathrm{S}h_\mathrm{N}^3 q$ becomes

$$\partial_t h = -\partial_x q, \qquad (4.2)$$

$$\mathcal{R}\,\partial_t q = \frac{5}{6}h - \frac{5}{2}\frac{q}{h^2} + \mathcal{R}\frac{9}{7}\frac{q^2}{h^2}\partial_x h - \mathcal{R}\frac{17}{7}\frac{q}{h}\partial_x q - \mathcal{C}\frac{5}{6}h\,\partial_x h + \frac{5}{6}h\,\partial_{xxx} h + \frac{5}{4}\frac{\mathcal{M}\,\mathcal{B}\,\partial_x h}{(1+\mathcal{B}\,h)^2}. \qquad (4.3)$$

Using (2.4), the relationships with the set of parameters (2.1) are

$$\mathcal{R} = (3\mathrm{Re})^{11/9}\,\mathrm{S}^{1/9}\,\mathrm{Ka}^{-1/3}, \qquad (4.4)$$

$$\mathcal{C} = (3\mathrm{Re})^{2/9}\,\mathrm{S}^{-8/9}\,\mathrm{Ka}^{-1/3}\,\sqrt{1-\mathrm{S}^2}, \qquad (4.5)$$

$$\mathcal{M} = (3\mathrm{Re})^{-4/9}\,\mathrm{S}^{-2/9}\,\mathrm{Ka}^{-1/3}\,\mathrm{Ma}, \qquad (4.6)$$

$$\mathcal{B} = (3\mathrm{Re})^{1/3}\,\mathrm{S}^{-1/3}\,\mathrm{Bi}. \qquad (4.7)$$

In this scaling, the Nusselt solution is $h = 1$ and the Hopf bifurcation is characterized by

$$k_\mathrm{c} = \left(\frac{2}{5}\mathcal{R} - \mathcal{C} + \frac{3}{2}\frac{\mathcal{M}\,\mathcal{B}}{(1+\mathcal{B})^2} \right)^{1/2}, \quad c_\mathrm{L} = 1 \quad \text{and} \quad Q_\mathrm{L} = -\frac{2}{3}. \qquad (4.8)$$

The wavenumber is rescaled as $k \to k/\mathcal{L}$. Note that Shkadov (1977) defined his reduced Reynolds number rather as $\delta = \mathcal{R}/45$. Remark also that rescaling time t by $\frac{1}{3}$ shows the equivalence between (4.1) and (1.2) for $\mathcal{C} = 0$ and $\mathcal{M} = 0$ when $\Phi = 2\mathcal{R}/5$ and $m = 6$.

4.2. *Vertical and isothermal films*

4.2.1. *Open and closed flows*

Figure 7 shows the stability diagram in the (k,$\mathcal{R}$)–plane for a vertically falling, isothermal film, *i.e.* $\mathcal{M} = \mathcal{C} = 0$. The solid line is the neutral curve k_c computed with (4.8). The dashed and dot-dashed lines are the blow-up boundaries computed using, respectively, the closed flow condition $\langle h \rangle_\xi = 1$ and the open flow condition $\langle h \rangle_\xi = (1/3 - Q)/c$, as defined with the new scaling. A major difference can be observed between both flow conditions. As displayed in the inset of figure 6, for the closed flow condition the Hopf bifurcation can become subcritical. For the open flow condition the Hopf bifurcation is supercritical for all $\mathcal{R}$. This implies that close to criticality the BE should always give bounded solutions with the open flow condition. However, figure 7 also shows that for $\mathcal{R} > \mathcal{R}_\mathrm{c}^*|_\mathrm{OP}$ the corresponding region of k is very small. The inset of this figure shows the blow-up boundary for open flow in the vicinity of $\mathcal{R}_\mathrm{c}^*|_\mathrm{OP}$.

The blow-up features as introduced in §3.2 can be now extracted from figure 7 as

$$\mathcal{R}_\mathrm{h}^* = 0.986, \qquad \mathcal{R}_\mathrm{c}^*|_\mathrm{CL} = 2.358 \qquad \text{and} \qquad \mathcal{R}_\mathrm{c}^*|_\mathrm{OP} = 5.401,$$

where the subscripts CL and OP indicate the corresponding flow condition. Note that since homoclines are solutions of infinite wavelength, they do not depend on the flow condition. To check for instance the blow-up features in the case of a water film at 20°C (see table 1) we use (4.4) to obtain the specific Reynolds numbers $\mathrm{Re}_\mathrm{h}^* = 3.0$, $\mathrm{Re}_\mathrm{c}^*|_\mathrm{CL} = 6.2$ and $\mathrm{Re}_\mathrm{c}^*|_\mathrm{OP} = 12.2$. It appears that the range of Re in which solutions are bounded is

larger with the open flow condition than with the closed one. Nevertheless, this bounding is conditional on the wavenumber, *i.e.* $k > k^*$. Also, no definitive conclusion can be drawn before addressing the accuracy and the stability of the stationary solutions.

4.2.2. *Accuracy of bounded solutions: BE versus WIBL*

The dotted line in figure 7 indicates the loci of bounded solutions of the BE where the amplitude exceeds by about 10% the one computed with the WIBL model. On this line, the phase speed is overestimated by about 20% with the BE. Interestingly, this boundary is approximately identical for both flow conditions. To the right of this boundary, the difference of the amplitudes of BE and WIBL model increases to reach about 100% at the respective blow-up boundaries. Even though the open flow condition gives bounded solutions for larger $\mathcal{R}$ than the closed flow condition, the wave amplitudes become much larger than for the WIBL model. So the 10%-accuracy limit is a good gauge for both flow conditions.

The 10%-accuracy limit approaches asymptotically the neutral stability curve. This can already be seen in figure 5 where for $\mathrm{Re} = 4, 5$ and 6 the discrepancy between the BE and the WIBL model becomes already large quite close to the Hopf bifurcation. The accuracy limit in figure 7 intersects the $\mathcal{R}$-axis at

$$\mathcal{R}_{\mathrm{h}}^{10\%} = 0.68,$$

which gives for water at 20°C to $\mathrm{Re} = 2.23$. The range of validity of the BE is therefore significatively reduced if the solutions are requested to be accurate.

Finally, using (4.4), we can also conclude that the range of validity of the BE – *i.e.* the range of Re for which solitary waves (homoclines) are bounded and accurate by less than 10% – increases with the Kapitza number as $\mathrm{Ka}^{3/11}$.

4.3. *Influence of inclination*

Figure 8 shows the stability diagram of the BE in the $(\mathcal{C}, \mathcal{R})$–plane computed with (4.1) for an isothermal film, *i.e.* $\mathcal{M} = 0$. The solid line corresponds to the neutral stability curve $k_{\mathrm{c}} = 0$, *i.e.* $\mathcal{C} = 2\mathcal{R}/5$, above which the flat film is stable, "**s**", and below which it is unstable, "**u**". The heavy dashed line indicates the boundary where homoclines blow up ($\mathcal{R}_{\mathrm{h}}^*$), whereas at the dashed and the long dashed lines all the linearly unstable modes blow up ($\mathcal{R}_{\mathrm{c}}^*$) for closed (CL) and nearly all for open (OP) flow conditions, respectively. The solutions in the region "$\mathbf{u}_k$" are bounded only in the range of wavenumbers $[k^*, k_{\mathrm{c}}]$ and unbounded in the range $[0, k^*]$. In the region "**b**" waves blow up unconditionally at any wavenumber (except very near threshold for open flow condition). Finally, the dotted line is the locus of the parameter $\mathcal{R}_{\mathrm{h}}^{10\%}$ defined in §4.2.2.

The dot-dashed lines in figure 8 correspond to fixed physical properties of some common liquids (see table 1) for two different inclinations of the wall, namely 10 and 30 degrees. These curves are computed by eliminating Re from $\mathcal{C}$ and $\mathcal{R}$ using (4.4,4.5). This leads to the relation

$$\mathcal{C} = \sqrt{1 - \mathrm{S}^2} \left(\frac{\mathcal{R}^2}{\mathrm{S}^{10}\mathrm{Ka}^3} \right)^{1/11}. \tag{4.9}$$

Increasing $\mathcal{C}$, *i.e.* decreasing S and/or Ka, reduces the range of validity of the BE in the linearly unstable domain.

Joo *et al.* (1991) have performed time-dependent simulations of the BE for isothermal falling films using the closed flow condition. Their figures 5-9 present the respective wave evolutions for increasing domain size, *i.e.* decreasing wavenumber. The parameters are $\beta = 45°$, $\mathrm{Re} = 1.179$, $\mathrm{Ka} = 4.386$ and $\mathrm{Ma} = 0$. This corresponds to $(\mathcal{R}, \mathcal{C}) = (2.751, 0.778)$

in the reduced scaling, *i.e.* to a point in the region "$\mathbf{u}_k|_{\mathrm{CL}}$" of figure 8 (see the plus sign) indicating that solutions are only bounded for $k > k^*$. It then agrees with travelling waves found in figures 5, 6 and 7 of Joo *et al.* (1991). On the contrary, figures 8 and 9 of their paper show 'catastrophic' behaviour, *i.e.* wave amplitudes growing 'explosively' in finite-time. Our explanation is that $k < k^*$ for these simulations. Using their scaling, the blow-up boundary is indeed at $k^*_{\mathrm{JDB}} = 1.236$. Therefore, the 'catastrophic behaviour' found by Joo *et al.* (1991) results from the blow-up character of the BE and is not associated to a secondary instability as conjectured by these authors. By coincidence, due to the choice of the parameter values in their paper, the transition for the secondary instability at $k_{\mathrm{s}} \approx k_{\mathrm{c}}/2$, found initially by Gjevik (1970) using weakly nonlinear analysis, is very close to the blow-up transition. Joo *et al.* (1991) also suggested that waves never equilibrate for $k < k_{\mathrm{s}}$. Yet, the present study shows that waves can be bounded in this region either for $\mathcal{R} < \mathcal{R}^*_{\mathrm{h}}$ or if $k > k^*$.

4.4. *Influence of Marangoni effect*

4.4.1. *Small Biot number limit:* $\mathrm{Bi} \ll 1$

For common liquids, the Biot number is usually ranged from 10^{-2} to 10^{-3} (see table 1 and appendix B). Therefore we can use the approximation

$$\frac{\mathcal{M}\,\mathcal{B}}{(1+\mathcal{B}\,h)^2} \approx \mathcal{M}\mathcal{B} \tag{4.10}$$

in (4.1) and (4.3) to study the Marangoni effect with $\mathcal{M}\mathcal{B}$ as a single parameter. In this limit, and looking at the generic equation (1.2), the Marangoni term behaves as a $m = 2$ term and does not lead to singularity.

Figure 9 represents the stability diagram of the BE in the $(\mathcal{M}\mathcal{B}, \mathcal{R})$–plane for a vertical wall, *i.e.* $\mathcal{C} = 0$. The legend is the same as for figure 8. Here, a range of unstable wavenumbers exists for all $\mathcal{R}$. The dot-dashed lines in figure 9 correspond as before to fixed liquid properties (table 1). They are calculated using

$$\mathcal{M}\mathcal{B} = \mathrm{Ma}\,\mathrm{Bi}\left(\frac{1}{\mathrm{S}^6\mathrm{Ka}^4\mathcal{R}}\right)^{1/11}, \tag{4.11}$$

obtained by eliminating Re from $\mathcal{M}\mathcal{B}$ and $\mathcal{R}$ with (4.4,4.6,4.7).

The domain of existence for homoclines nearly vanishes for large $\mathcal{M}\mathcal{B}$. However, as indicated in table 1, the product MaBi remains small for common liquids (Scheid *et al.* 2002). For instance, for a vertically falling water film at 20°C the value MaBi = 2 corresponds to $\Delta T = 28K$ when $\alpha = 100W/m^2K$. In this case, the BE can be used with satisfactory accuracy up to $\mathrm{Re} = 1.8$ ($\mathcal{R}^{10\%}_{\mathrm{h}} = 0.52$).

Joo *et al.* (1991) have performed time-dependent simulations of the BE for large Biot number. Considering the case of figure 14 in their paper, for $\beta = 45°$, $\mathrm{Re} = 1.179$, $\mathrm{Ka} = 4.386$, $\mathrm{Ma} = 11.696$ and $\mathrm{Bi} = 5.848$, they observed blow-up of the travelling wave. This result is expected given that solutions blow-up even for $\mathrm{Ma} = 0$ (see the plus sign in figure 8), and that the Marangoni effect further decreases the validity domain (see figure 9). Nevertheless, a region (even small) possessing bounded solutions is always present, *i.e.* whatever the value of $\mathcal{M}\mathcal{B}$.

4.4.2. *Subcritical behaviour of the Benney equation*

For the isothermal case we have seen in figure 5 that the Hopf bifurcation computed with the BE is always subcritical for $\mathrm{Re} > \mathrm{Re}^*_{\mathrm{c}}$. However, the bifurcation becomes already subcritical even slightly before $\mathrm{Re}^*_{\mathrm{c}}$ as shown by the inset of figure 6: in the sub-domain

bounded from below by the solid line and by the dashed curves otherwise, the family of solutions has not only one but two saddle-nodes or turning points. Pumir *et al.* (1983) have shown that the blow-up of the BE is linked to the absence of homoclinic solutions. We have furthermore shown that the subcritical bifurcation is related to the absence of all solutions in the unstable range of wavenumbers. In this sense, the subcritical behavior is non-physical as far as isothermal conditions are concerned. We thus analyse here how this behavior is influenced by the Marangoni effect and whether the subcritical bifurcation in this case has a physical meaning.

Figure 10 displays the stability diagram for different values of $\mathcal{MB}$ for closed (dashed lines) and open (dot-dashed lines) flow conditions. The corresponding neutral stability curves are plotted as dotted lines. The figure shows that for closed flow the sub-domain where subcritical bifurcations are found extends towards smaller $\mathcal{R} < \mathcal{R}_c^*$ for increasing $\mathcal{MB}$. A somehow similar observation is made also for the open flow condition. Although there the Hopf bifurcation is always supercritical, the family has an additional turning point slightly above the bifurcation, as illustrated by the inset of figure 10. The resulting three turning points allow for a similar shape of the large amplitude part of the bifurcation diagram as for the closed flow condition. Notice that no difference was observed in the curves of figure 10 when dispensing with the small Biot number limit approximation (4.10), still using the common values of the Biot number as indicated in table 1.

Now, we can raise the question, is this subcritical behavior physical with the Marangoni effect? Actually, for horizontal layer, VanHook *et al.* (1997) found that the Marangoni instability is subcritical and predicts a blow-up of the solution. However, as pointed out by Kalliadasis *et al.* (2003*a*), this is not a true singularity formation, as forces of non-hydrodynamic origin, namely van der Waals forces not included here, become increasingly important in the region of very thin films and will arrest this blow-up behaviour. Kalliadasis *et al.* (2003*a*) have also shown that the dry patch formation is associated to a divergence of the characteristics (amplitude, phase speed) of the solutions but is not associated to the absence of solution. Therefore, we can state that the subcritical behaviour of the Benney equation including the Marangoni effect described above is unphysical, in contrast to the subcritical instabilities known for horizontal planes. Let us give two more arguments in this direction: (i) the dry patch formation is obviously linked to the Marangoni effect and does not appear in the isothermal case; yet, the boundaries in figure 10 are obtained by continuation from the isothermal case, and we know that the subcritical bifurcation in the isothermal case is unphysical. (ii) we find that for vertically falling films, our reference model (WIBL) *does never* yield subcritical behaviour. This is illustrated in the inset of figure 10 by the thin lines.

Remark that in the case of the closed flow condition, figure 10 indicates that the bifurcation is subcritical for all $\mathcal{R}$ when

$$\mathcal{MB} \approx 1.$$

This implies that above this value for $\mathcal{MB}$ the Benney equation fails to describe the physics for vertically falling films even close to criticality.

5. Stability of stationary solutions

This section analyses the two-dimensional stability of the stationary one-hump solutions discussed up to now. We focus especially on the range $[\mathcal{R}_h^*, \mathcal{R}_c^*]$ where only part of the linearly unstable modes results in bounded stationary solutions. We will determine the stability of those solutions to disturbances of larger period that may induce the coalescence of humps. This is done performing a Floquet analysis following, for instance,

Chang *et al.* (1993). Let $h_0(\xi)$ be the travelling-wave solution of wavenumber k. Then the film thickness h is written as the superposition of this solution and a small disturbance

$$h = h_0(\xi) + \eta h_1(\xi) \exp\{\mathrm{i}\varsigma k\xi + st\}, \tag{5.1}$$

where $\eta \ll 1$ and h_1 is a real function with the same period as h_0; $s = s_r + \mathrm{i}s_i$ where the real part s_r corresponds to the growth rate of the disturbance and the imaginary part s_i to the relative phase velocity. The detuning parameter ς represents the ratio of the wavenumber of the disturbance and the one of the travelling-wave solution $h_0(\xi)$. For $\varsigma = 0$ the instability has the same wavelength as the wave, and for $0 < \varsigma \leq \frac{1}{2}$ the instability is *sub-harmonic*. It is called *side-band* when ς is close to zero (Chang *et al.* 1994). For instance, $\varsigma = \frac{1}{2}$ implies that the disturbance has twice the period of the wave. Substituting (5.1) into (2.2) and linearizing in η amounts to solve an eigenvalue problem of the form $sh_1 = L(h_0, c, Q, \varsigma)h_1$ where L is a linear operator.

Figure 11 shows the growth rate "$\max(s_r)$" of the most amplified disturbance and the corresponding detuning parameter $\varsigma_{\max}$ versus the wavenumber of travelling-wave solutions, for $\mathcal{R} = 1.5$ and 3, with $\mathcal{C} = \mathcal{M} = 0$. The heavy and thin lines result from the BE and WIBL model, respectively, whereas solid and dashed lines stand for closed and open flow condition, respectively. The blow-up boundary at k^* is indicated by an asterisk and the neutral mode by the letter "c". The blow-up features of the stationary solutions analysed here can be found in figure 7. For the value of $\mathcal{R}$ considered, the growth rate $\max(s_r)$ is positive for all k implying that none of the bounded solutions emerging from the Hopf bifurcation is stable to sub-harmonic disturbances. If the imaginary part of s (not shown in figure 11) is equal to zero the waves coalesce steadily by a relative translation of the humps and by volume transfer between the humps (Chang *et al.* 1995). This is the case for the WIBL model. In contrast, for the BE the imaginary part of s is non-zero. This indicates that the instability leads to oscillating behaviour that may or may not lead to coalescence. Only time-dependent simulations of the BE can clarify this point. An example is presented in figure 12. Two periods of a stationary solution calculated with the closed flow condition and corresponding to the point $(\mathcal{R}, k) = (1.5, 0.5)$ in figure 7 with additional noise are used as initial condition. The time series for the amplitude at a fixed point in space (figure 12) shows that the ongoing process comprises growing sinusoidal oscillations of the relative amplitudes of the two humps that lead to a coalescence mediated finite-time blow-up. We propose to call this type of coalescence *oscillation mediated coalescence* (see also Bestehorn *et al.* (2003)).

The results of the stability analysis are important because physically relevant domains are always at least twice larger than the wavelength of the stationary solution. Thereby, sub-harmonics will always develop, and for $\mathcal{R} \geq \mathcal{R}_h^*$, blow-up will be promoted by coalescence as illustrated above in figure 12. For instance, looking at the blow-up boundary for the closed flow condition in figure 7, at any $\mathcal{R}$ larger than $\sim$1.4, a bounded one-hump travelling-wave solution put twice in a domain of doubled size is unstable and yields finite-time blow-up. The same happens for the open flow condition, at any $\mathcal{R}$ larger than $\sim$1.8. In conclusion, even thought the Benney equation gives bounded solutions beyond the blow-up boundary for homoclines $\mathcal{R}_{\mathrm{h}}^*$, those solutions should be considered with special care, furthermore independently of the flow condition.

6. Concluding remarks

The Benney equation has been investigated including the effect of surface tension, wall inclination and thermocapillarity. We focused on the validity of travelling-wave solutions in terms of accuracy and finite-time blow-up. The accuracy was checked by comparison

with a reference model developed by Ruyer-Quil & Manneville (2000, 2002), to which we added the Marangoni effect. This model was shown to agree with the Benney equation at low Reynolds number where the exact long-wave expansion is known to apply.

We have established in this paper the equivalence between the boundary beyond which the dynamical system associated to the Benney equation has no travelling-wave solutions and the boundary for finite-time blow-up obtained in simulations by Oron & Gottlieb (2002). The solutions that tend to blow up first, *i.e.* at the smallest Reynolds number, were found to be the one-hump solitary waves, that correspond to homoclinic orbits of the associated dynamical system. These solutions are identical for closed and open flow conditions. For vertically falling isothermal films these one-hump solitary waves are bounded only if $\mathrm{Re} < 0.330\,\mathrm{Ka}^{3/11}$. Furthermore, the accuracy of their amplitudes is below 10% for $\mathrm{Re} < 0.243\,\mathrm{Ka}^{3/11}$. The accuracy and blow-up boundaries were also computed for solutions of finite wavelength above the linear stability threshold. We defined and determined a third limiting Reynolds number above which none of the linearly unstable modes is bounded for the closed flow condition. For the open flow condition only a narrow range of linearly unstable modes leads to bounded solutions above this value. We reduced by two the number of independent parameters by rescaling the Benney equation and taking the small Biot number limit, which is confirmed by experimental evidence (Kabov *et al.* 1996, see also appendix B). This enabled us to study exhaustively the influence of inclination and thermocapillarity on the accuracy and blow-up boundaries. Both effects narrow the range of Reynolds numbers in which the Benney equation is applicable as summarized in figures 8 and 9.

We paid particular attention to the flow condition that can correspond either to closed or open flow. While the former is widely used in literature, only the latter coincides with realistic experimental conditions. For the open flow condition the validity domain of the Benney equation is larger than for the closed flow condition.

In this paper, we have accurately demonstrated for the Benney equation the link between absence-of-solution and blow-up boundaries for the closed flow condition. For the open flow condition, this link is just conjectured and should be addressed in a future work. In the same vein, weakly nonlinear analysis of the Benney equation for the closed flow condition is classical and provides, for instance, the transition between supercritical and subcritical bifurcations at $\mathcal{R} > 5/12^{1/3} \approx 2.184$ for isothermal and vertical films (see figure 7 and Oron & Gottlieb (2004)). On the contrary, weakly nonlinear analysis in the case of open flow has not been yet been realized up to now. We therefore rely on our numerical findings.

In the isothermal case and with the open flow condition the Hopf bifurcation is always supercritical while with the closed flow condition, the Hopf bifurcation becomes subcritical above the Reynolds number at which none of the linearly unstable modes is bounded. This subcritical bifurcation is shown to be an anomaly of the Benney equation and therefore unphysical, even for the heated case. In this latter case, we even found that above $\mathcal{MB} \approx 1$, all the bounded solutions emerge by subcritical bifurcation so that the Benney equation is totally inapplicable.

We did not vary simultaneously the strength of the Marangoni effect and the wall inclination. However, combining our results with the ones of Thiele & Knobloch (2004) indicates that the subcritical behaviour of the Benney equation can become physically meaningful for very small or vanishing inclination angles only. However, then $\mathrm{Re} \ll 1$ and the Benney term $\approx \partial_x(h^6 \partial_x h)$ may be neglected, what cures any singularity.

The results of numerical simulations performed by Joo *et al.* (1991) have been recovered by our analysis. We could explain and predict the 'dramatic behaviour' observed in that

work. Actually, it results from the blow-up character of the Benney equation and is not associated to a secondary instability as conjectured by these authors.

The stability of stationary solutions has also been addressed for solutions that are conditionally bounded depending on the wavenumber. They were all found to be unstable to disturbances of higher periodicity. This gives the possibility to the sub-harmonics to develop and as a consequence yields finite-time blow-up. This was illustrated by numerical simulations that show blow-up promoted by wave coalescence.

At this stage, let us present a time-dependent simulation of the Benney equation (4.1) obtained using a finite-difference implicit scheme. Figure 13 displays the nonlinear response of a vertically falling and isothermal film submitted to a periodic forcing with small noise at the inlet (left border). The reduced Reynolds number $\mathcal{R} = 0.9$ has been chosen to lie below $\mathcal{R}_{\rm h}^*$, *i.e.* the blow-up of homoclines. It is of main interest to observe that at a given position, still a singularity appears in a finite-time, leading to the blow-up of the film thickness. The blow-up is preceeded by a succession of coalescence between adjacent travelling waves. We think that the local coalescence of humps in an extended system induces a local increase of the flow rate that locally "pushes" the system beyond the blow-up boundary in the stability diagram of figure 7. In conclusion, special care has to be taken since blow-up of travelling waves may occur even slightly below to the blow-up boundary presented here.

As one advantage, the Benney equation allows to describe with a single evolution equation the different physical effects in a falling film, namely in our case, viscosity, gravity, surface tension and thermocapillarity. We believe, this ensures that the Benney equation will remain a helpful model to study thin film flows, especially to identify new phenomena but also in a limited parameter range for quantitative predictions. Actually, many other effects may be added to the Benney equation like evaporation (Joo *et al.* 1991), Van der Waals force (Tan *et al.* 1966), chemical reaction (Trevelyan *et al.* 2002), topolographical effects (Kalliadasis *et al.* 2000), non-uniform heating (Miladinova *et al.* 2002; Kabov *et al.* 2001; Scheid *et al.* 2002; Skotheim *et al.* 2002; Kalliadasis *et al.* 2003*b*), etc. The validity of the Benney equation should in the future also be addressed including these additional effects.

Finally, The integral boundary layer model used in this work as the reference model does not suffer from singular behaviour and is accurate for larger Reynolds number than the Benney equation Ruyer-Quil & Manneville (2000, 2002). Furthermore, the study of stationary solutions with the WIBL model does not require much supplementary effort than the BE. So although for the ranges of validity defined in this paper, the BE can be used safely, the WIBL represents a promising alternative.

Acknowledgments

The authors gratefully acknowledge fruitful discussions with Manuel G. Velarde, Alex Oron and Paul Manneville. This work has been facilitated by the cooperation between the CNRS-CGRI-FNRS. B.S. thanks the FAST laboratory for hospitality during the visit there, made possible by a Marie-Curie grant of the European Union (contract HPMT-CT-2000-00207). P.C. acknowledges financial support of the "Fonds National de la Recherche Scientifique" (Belgium).

Appendix A. Derivation of the Weighted Integral Boundary Layer (WIBL) model

The main assumption behind the boundary layer approximation is the smallness of the film thickness modulations as compared to the film thickness itself. We introduce a formal parameter $\varepsilon \ll 1$ and apply a gradient expansion through the transformation $\partial_t \to \varepsilon\partial_t$ and $\partial_x \to \varepsilon\partial_x$ to the governing equations. Therefore, up to first-order in ε the pressure gradient can easily be eliminated (Shkadov 1967) and the two-dimensional dimensionless boundary layer equations, respectively, the momentum, energy and continuity equations, read

$$\varepsilon(\partial_t u + u\,\partial_x u + v\,\partial_y u) - \partial_{yy} u - \mathrm{S} + \varepsilon(\sqrt{1-\mathrm{S}^2}\,\partial_x h - \mathrm{Ka}\,\partial_{xxx} h) = 0, \tag{A 1}$$

$$\varepsilon(\partial_t T + u\,\partial_x T + v\,\partial_y T) - \frac{1}{\mathrm{Pr}}\partial_{yy} T = 0, \tag{A 2}$$

$$\partial_x u + \partial_y v = 0, \tag{A 3}$$

where u is the streamwise velocity, v the cross-stream velocity, T the temperature and $\mathrm{Pr} = \nu/\chi$ the Prandtl number with χ the thermal diffusivity. The boundary conditions at the free surface $y = h(x,t)$ are the kinematic condition, the balance of tangential stress and the Newton's cooling law which read, at first-order in ε, respectively,

$$v = \partial_t h + u\,\partial_x h, \tag{A 4}$$

$$\partial_y u = -\varepsilon \mathrm{Ma}\,\partial_x T^{(s)}, \tag{A 5}$$

$$\partial_y T = -\mathrm{Bi}\,T^{(s)}, \tag{A 6}$$

where $T^{(s)} \equiv T(x, h(x,t), t)$ is the temperature at the free surface. At the wall $y = 0$ the no-slip condition and the constant temperature are imposed as

$$u = v = 0\,, \tag{A 7}$$

$$T = 1\,. \tag{A 8}$$

Now, the main goal of the integral boundary layer approach is the elimination of the cross-stream coordinate y. Following Kapitza & Kapitza (1949) and Shkadov (1967), the simplest idea would be to assume a parabolic velocity profile

$$u = 3\frac{q}{h}\left(\frac{y}{h} - \frac{1}{2}\left(\frac{y}{h}\right)^2\right), \tag{A 9}$$

where q is the local flow rate. Shkadov suggested to extend this assumption by expanding the velocity field on a basis of self-similar profiles $u = \sum a_i(x,t) f_i(y/h)$. This idea was re-investigated by Ruyer-Quil & Manneville (2002) using polynomial test functions f_i. They derived an averaged momentum equation at first order and showed that increasing the number of polynomials or selecting different weight functions eventually leads to the same averaged momentum equation. They actually proved that the Galerkin method gives the results with minimal algebraic manipulations. It consists in integrating the momentum equation (A 1) with the test function as the weight function itself, namely $y/h - (y/h)^2/2$, having substituted the velocity profiles u and v given by (A 9) and (A 3). Moreover, the integration of the continuity equation (A 3) across the film, using (A 9) gives the mass balance of the film

$$\partial_t h + \partial_x q = 0. \tag{A 10}$$

The study performed by Ruyer-Quil and Manneville can be extended without difficulty to the set (A 1-A 8). Using (A 10) to identify $\partial_t h = -\partial_x q$, the momentum equation becomes

$$\frac{5}{6}\mathrm{S}h - \frac{5}{2}\frac{q}{h^2} = \varepsilon\left(\partial_t q - \frac{9}{7}\frac{q^2}{h^2}\partial_x h + \frac{17}{7}\frac{q}{h}\partial_x q + \frac{5}{6}\sqrt{1-\mathrm{S}^2}h\,\partial_x h \right.$$
$$\left. -\frac{5}{6}\mathrm{Ka}\,h\,\partial_{xxx}h - \frac{5}{4}\mathrm{Ma}\partial_x T^{(s)}\right), \tag{A 11}$$

whose solution at leading order ($\varepsilon \to 0$) is

$$q = \mathrm{S}\frac{h^3}{3}. \tag{A 12}$$

The surface temperature $T^{(s)}$ appears in a term already at ε-order. It is therefore enough to get its approximation at leading order. Solving $\partial_{yy}T = 0$ together with the boundary conditions (A 6) and (A 8) and taking $y = h$ leads to the expression

$$T^{(s)} = \frac{1}{1+\mathrm{Bi}\,h}. \tag{A 13}$$

We can now substitute (A 13) into (A 11) and write the first-order weighted integral boundary layer model (WIBL) with Marangoni effect

$$\partial_t h = -\partial_x q, \tag{A 14a}$$

$$\partial_t q = \frac{5}{6}\mathrm{S}h - \frac{5}{2}\frac{q}{h^2} + \frac{9}{7}\frac{q^2}{h^2}\partial_x h - \frac{17}{7}\frac{q}{h}\partial_x q - \frac{5}{6}\sqrt{1-\mathrm{S}^2}h\,\partial_x h + \frac{5}{6}\mathrm{Ka}\,h\,\partial_{xxx}h$$
$$+\frac{5}{4}\frac{\mathrm{Ma}\,\mathrm{Bi}\,\partial_x h}{(1+\mathrm{Bi}\,h)^2}, \tag{A 14b}$$

where we dropped the formal parameter ε.

Additionally, we can define $q = q^{(0)} + q^{(1)}$, where the superscript denotes the order in x-differentiation, assume $\varepsilon^2\mathrm{Ka} = O(1)$ and perform a long-wave expansion of the system (A 14). Substituting $-\partial_x q^{(0)}$ to $\partial_t h$, we get

$$q^{(0)} = \mathrm{S}\frac{h^3}{3}, \tag{A 15}$$

$$q^{(1)} = \left(\frac{2}{15}\mathrm{S}^2h^6 - \sqrt{1-\mathrm{S}^2}\,\frac{h^3}{3} + \frac{h^2}{2}\frac{\mathrm{Bi}\,\mathrm{Ma}}{(1+\mathrm{Bi}\,h)^2}\right)\partial_x h + \mathrm{Ka}\frac{h^3}{3}\partial_{xxx}h, \tag{A 16}$$

whose substitution into the conservation equation (A 10) leads back to the BE (2.2). It therefore shows that the WIBL model is an intermediate model between the boundary layer model and the BE. Therefore the former should contain at least all the physics of the latter.

Appendix B. Small Biot number: analogy with forced convection

Up to now, we imposed an arbitrary value for the Biot number based on the assumption that the heat transfer coefficient at the liquid-gas interface is small. Let us now justify this assumption by considering the classical problem of forced convection along a heated plate (see *e.g.* Holman (1989)). The boundary layer theory in this case yields an expression for the Nusselt number

$$\mathrm{Nu}_L = \frac{\alpha L}{k} = 0.664\mathrm{Re}_L^{1/2}\mathrm{Pr}^{1/3}, \tag{B 1}$$

which quantifies the heat transfer from the plate to the fluid layer; L is the length of the heated plate and $\mathrm{Re}_L = U_\infty L/\nu$ where U_∞ is the relative velocity between the plate and

the fluid. We shall now make the following analogy: let the air be the fluid and the liquid film (assumed to be flat for simplicity) be the 'plate' in our forced convection problem; this 'plate' moving at the film surface velocity. The typical characteristic temperature difference between the film surface and the air far from the interface is about $10K$. Typical value of the film surface velocity is $U_\infty = 10\,cm/s$. Setting for instance $L = 10\,cm$ as the length of the heater, we are able to estimate the heat transfer coefficient at the liquid-gas interface, provided that the ambient air is at 22°C and that the air properties are given at 'the average boundary layer temperature' (defined as the arithmetic mean between the 'plate' and the ambient air). Then, $\nu_{\rm air} = 15.69 \times 10^{-6}\,m^2/s$, $k_{\rm air} = 0.02624\,W/mK$ and $\Pr = 0.708$ at the air temperature of $300K$. The heat transfer coefficient, using (B 1), reads therefore

$$\alpha = 3.92 \left(\frac{U_\infty}{L}\right)^{1/2} \approx 4\,W/m^2K, \tag{B 2}$$

As expected, the basic value of the heat transfer coefficient at the liquid-gas interface is very small. Nevertheless, our approximation underestimates the effective heat transfer at the liquid-gas interface that is generally improved by wave motion and residual evaporation. These effects may increase by one or several order of magnitude the heat transfer coefficient. For this reason, we overestimated arbitrarily α up to $100W/m^2K$ to calculate Biot numbers for usual liquids given in table 1.

REFERENCES

Alekseenko, S., Nakoryakov, V. & Pokusaev, B. 1985 Wave formation on a vertical falling liquid film. *AIChE J.* **1446-1460**, 31.

Alekseenko, S., Nakoryakov, V. & Pokusaev, B. 1994 *Wave flow in liquid films*, 3rd edn. Begell House.

Benney, D. 1966 Long waves on liquid films. *J. Math. Phys. (N.Y.)* **45**, 150.

Bertozzi, A. & Pugh, M. 1998 Long-wave instabilities and saturation in thin film equations. *Comm. Pure Appl. Math.* **51**, 625.

Bestehorn, M., Pototsky, A. & Thiele, U. 2003 3D large scale Marangoni convection in liquid films. *Eur. Phys. J. B* **33**, 457–467.

Boos, W. & Thess, A. 1999 Cascade of structures in long-wavelength Marangoni instability. *Phys. Fluids* **11**, 1633.

Chang, H. 1994 Wave evolution on a falling film. *Ann. Rev. Fluid Mech.* **26**, 103.

Chang, H.-C., Cheng, M., Demekhin, E. & Kopelevitch, D. 1994 Secondary and tertiary excitation of three-dimensional patterns on a falling films. *J. Fluid Mech.* **270**, 251–275.

Chang, H.-C. & Demekhin, E. 2002 *Complex wave dynamics on thin films*. Elsevier, D. Möbius and R. Miller.

Chang, H.-C., Demekhin, E. & Kalaidin, E. 1995 Interaction dynamics of a solitary waves on a falling film. *J. Fluid Mech.* **294**, 123.

Chang, H.-C., Demekhin, E. & Kopelevitch, D. 1993 Nonlinear evolution of waves on a vertically falling film. *J. Fluid Mech.* **250**, 433.

Colinet, P., Legros, J. & Velarde, M. 2001 *Nonlinear Dynamics of Surface-Tension-Driven Instabilities*. Wiley-VCH.

Doedel, E., Champneys, A., Fairfrieve, T., Kuznetsov, Y., Sandstede, B. & Wang, X. 1997 Auto 97 continuation and bifurcation software for ordinary differential equations. *Montreal Concordia University* .

Doedel, E., Keller, H. B. & Kernevez, J. P. 1991*a* Numerical analysis and control of bifurcation problems (I) Bifurcation in finite dimensions. *Int. J. Bifurcation Chaos* **1**, 493–520.

Doedel, E., Keller, H. B. & Kernevez, J. P. 1991*b* Numerical analysis and control of bifurcation problems (II) Bifurcation in infinite dimensions. *Int. J. Bifurcation and Chaos* **1**, 745–72.

Drazin, P. 1992 *Nonlinear systems*. Cambridge University Press.

Gjevik, B. 1970 Occurrence of finite-amplitude surface waves on falling liquid films. *Phys. Fluids* **13**, 1918.

Goussis, D. & Kelly, R. 1991 Surface wave and thermocapillary instabilities in a liquid film flow. *Journal of Fluid Mechanics* **223**, 25.

Hocherman, T. & Rosenau, P. 1993 On KS-type equations describing the evolution and rupture of a liquid interface. *Physica D* **67**, 113.

Holman, J. 1989 *Heat Transfer*. Mc Graw-Hill.

Huerre, P. & Rossi, M. 1998 *Hydrodynamics and nonlinear instabilities*. C. Godrèche and P. Manneville, Cambridge University Press.

Joo, S., Davis, S. & Bankoff, S. 1991 Long-wave instabilities of heated falling films two-dimensional theory of uniform layers. *J. Fluid Mech.* **230**, 117.

Joo, S., Davis, S. & Bankoff, S. 1996 A mechanism for rivulet formation in heated falling films. *J. Fluid Mech.* **321**, 279.

Kabov, O. & Chinnov, E. 1997 Heat transfer from a local heat source to a subcooled falling liquid film evaporating in a vapor-gas medium. *Russ. J. Eng. Thermophys.* **7**, 1.

Kabov, O., Marchuk, I. & Chupin, V. 1996 Thermal imaging study of the liquid film flowing on vertical surface with local heat source. *Russ. J. Eng. Thermophys.* **6**, 105.

Kabov, O., Scheid, B., Marchuk, I. & Legros, J. 2001 Free surface deformation by thermocapillary convection in a flowing locally heated thin liquid layer. *Mekh. Zhi. Gaza* **3**, 200.

Kabov, O., Scheid, B., Sharina, I. & Legros, J. 2002 Heat transfer and rivulet structures formation in a falling thin liquid film locally heated. *Int. J. Therm. Sci.* **41**, 664.

Kalliadasis, S., Bielarz, C. & Homsy, G. 2000 Steady free-surface thin film flows over topography. *Phys. Fluids* **12**, 1889.

Kalliadasis, S., Demekhin, E., Ruyer-Quil, C. & Velarde, M. 2003*a* Thermocapillary instability and wave formation on a film flowing down a uniformly heated plane. *J. Fluid Mechanics* **492**, 303–338.

Kalliadasis, S., Kiyashko, A. & Demekhin, E. 2003*b* Marangoni instability of a thin liquid film heated from below by a local heat source. *J. Fluid Mech.* **475**, 377–408.

Kapitza, P. & Kapitza, S. 1949 Wave flow of thin layers of a viscous fluid. *Zh. Ekper. Teor. Fiz.* **19**, 105.

Keller, H. 1977 *Numerical solution of bifurcation and nonlinear eigenvalue problems*, 3rd edn. Applications of bifurcation theory, Rabinowitz P. H.

Krishnamoorthy, S. & Ramaswamy, B. 1995 Spontaneous rupture of thin liquid films due to thermocapillarity: A full-scale direct numerical simulation. *Phys. Fluids* **7**, 2291.

Lin, S. 1974 Finite amplitude side-band stability of a viscous fluid. *J. Fluid Mech.* **63**, 417.

Liu, J. & Gollub, J. 1994 Solitary wave dynamics of film flows. *Phys. Fluids* **6**, 1702.

Liu, J., Paul, J. & Gollub, J. 1993 Measurements of the primary instabilities of film flows. *J. Fluid Mech.* **250**, 69.

Liu, J., Schneider, J. & Gollub, J. 1995 Three-dimensional instabilities of film flows. *Physics of Fluids* **7**, 55.

Miladinova, S., Slavtchev, S., Lebon, G. & Legros, J. 2002 Long-wave instabilities of non-uniformly heated falling films. *J. Fluid Mech.* **453**, 153.

Nusselt, W. 1916 Die oberflachenkondensation des wasserdampfes. *Z. VDI* **50**, 541.

Ooshida, T. 1999 Surface equation of falling film flows with moderate Reynolds number and large but finite weber number. *Phys. Fluids* **11**, 3247.

Oron, A. 2000 Nonlinear dynamics of three-dimensional long-wave Marangoni instability in thin liquid films. *Phys. Fluids* **12**, 1633.

Oron, A., Davis, S. & Bankoff, S. 1997 Long-scale evolution of thin liquid films. *Rev. Mod. Phys.* **69**, 931.

Oron, A. & Gottlieb, O. 2002 Nonlinear dynamics of temporally excited falling liquid films. *Phys. Fluids* **14**, 2622.

Oron, A. & Gottlieb, O. 2004 Subcritical and supercritical bifurcations of the first- and second- order benney equations. *In press to J. Eng. Math.* .

Pearson, J. 1958 On convection cells induced by surface tension. *J. Fluid Mech.* **4**, 489.

Pumir, A., Manneville, P. & Pomeau, Y. 1983 On solitary waves running down an inclined plane. *J. Fluid Mech.* **135**, 27.

Ramaswamy, B., Chippada, S. & Joo, S. 1996 A full-scale numerical study of interfacial instabilities in thin-film flows. *J. Fluid Mech.* **325**, 163.

Ramaswamy, B., Krishnamoorthy, S. & Joo, S. W. 1997 Three-dimensional simulation of instabilities and rivulet formation in heated falling films. *J. Comp. Phys.* **131**, 70.

Rosenau, P., Oron, A. & Hyman, J. 1992 Bounded and unbounded patterns of the Benney equation. *Phys. Fluids A* **4 (6)**, 1102.

Ruyer-Quil, C. & Manneville, P. 2000 Improved modeling of flows down inclined planes. *Eur. Phys. J. B* **15**, 357.

Ruyer-Quil, C. & Manneville, P. 2002 Further accuracy and convergence results on the modeling of flows down inclined planes by weighted-residual approximations. *Phys. Fluids* **14**, 170.

Salamon, T., Armstrong, R. & Brown, R. 1994 Traveling waves on vertical films: Numerical analysis using the finite element method. *Phys. Fluids* **5**, 2202.

Scheid, B., Oron, A., Colinet, P., Thiele, U. & Legros, J. 2002 Nonlinear evolution of non-uniformly heated falling liquid films. *Phys. Fluids* **14**, 4130.

Scriven, L. & Sterling, C. 1964 On cellular convection driven surface tension gradients: effects of mean surface tension and surface viscosity. *J. Fluid Mech.* **19**, 321.

Shkadov, V. 1967 Wave flow regimes of a thin layer of viscous fluid subject to gravity. *Isv. Akad. Nauk SSSR* **2**, 43.

Shkadov, V. 1977 Solitary waves in a viscous film. *Isv. Akad. Nauk SSSR* **1**, 63.

Skotheim, J., Thiele, U. & Scheid, B. 2002 On the instability of a falling film due to localized heating. *J. Fluid Mech.* **475**, 1.

Smith, K. 1966 On convective instability induced by surface gradients. *J. Fluid Mech.* **24**, 401–414.

Tan, M. J., Bankoff, S. G. & Davis, S. H. 1966 Steady thermocapillary flows of thin liquid layers. *Phys. Fluids A* **2**, 313.

Thiele, U. & Knobloch, E. 2004 Thin liquid films on a slightly inclined heated plate. *Physica D* **190**, 213–248.

Thiele, U., Neuffer, K., Bestehorn, M., Pomeau, Y. & Velarde, M. G. 2002 Sliding drops on an inclined plane. *Colloid Surf. A* **206**, 87–104.

Thiele, U., Velarde, M. G., Neuffer, K., Bestehorn, M. & Pomeau, Y. 2001 Sliding drops in the diffuse interface model coupled to hydrodynamics. *Phys. Rev. E* **64**, 061601, 1–12.

Trevelyan, P., Kalliadasis, S., Merkin, J. & Scott, S. 2002 Dynamics of a vertically falling film in the presence of a first chemical reaction. *Phys. Fluids* **14**, 2402.

VanHook, S., Schatz, M., Swift, J., McCormick, W. & Swinney, H. 1997 Long wavelength surface-tension-driven Bénard convection: Experiment and theory. *J. Fluid Mech.* **345**, 45.

Weast, R. & Selby, S. 1966 *Handbook of Chemistry and Physics*, 63^{th} edn. The Chemical Rubber CO.

Yih, C. 1955 Stability of two-dimensional parallel flows for three dimensional disturbances. *Quart. Appl. Math.* **12**, 434.

Yih, C. 1963 Stability of liquid flow down an inclined plane. *Phys. Fluids* **6**, 321.

Liquid	l_ν (μm)	t_ν (ms)	Ka	$\mathrm{Ma}\vert_{\Delta T=1K}$	$\mathrm{Bi}\vert_{\alpha=100W/m^2K}$
Water at 20°C	47	2.2	3375	8.9	0.008
Water at 15°C	50	2.3	2950	7.7	0.009
FC-72 at 20°C	26	1.6	1100	9.7	0.045
MD-3F at 30°C	31	1.8	703	5.8	0.047
25%-Ethyl alcohol at 20°C	87	3.0	500	1.5	0.02

TABLE 1. Rounded values of characteristic liquid parameters (Weast & Selby 1966). Those liquids are effectively used in experiments (Kabov *et al.* 1996; Kabov & Chinnov 1997). See appendix B for the value of α.

Figure 1. Sketch of a thin film flowing down a heated inclined wall.

Figure 2. Maximum thickness of travelling-wave solutions $h_{\max}/h_{\rm N}$ as a function of Re, computed with the BE (dashed curve) and the WIBL model (dot-dashed curve) under the closed flow condition for a film falling on a vertical (S = 1) and isothermal (Ma = 0) wall; We = 1000 and $\varepsilon_L = 0.04/2\pi$. For comparison, results of the Navier-Stokes equations (solid curve) obtained by Salamon *et al.* (1994) as well as results from time-dependent simulations of the BE (circles) obtained by Oron & Gottlieb (2002) are displayed.

Figure 3. Bifurcation diagram showing the phase speed $c/c_{\rm L}$ and maximal amplitude $h_{\max}/h_{\rm N}$ of travelling-wave solutions versus wavenumber k. The parameters are S = 1, Ma = 0 (vertical and isothermal wall), Re = 2.0667 and Ka = 3375. The closed flow condition is imposed. The solid (resp. dashed) lines are families obtained with the BE (resp. WIBL model). The γ_2 families correspond to fast one-hump waves and γ_1 ones to slow one-hole waves, as illustrated by the two corresponding insets. The arrows and letters refer to solutions plotted in figure 4. HB: Hopf Bifurcation - PD: Period Doubling - IP: Intersection Point. The HB bifurcates from the Nusselt flat film solution while the PD bifurcates from the families of $n = 2$ subharmonic solutions (not drawn on the figure).

Figure 4. Profiles of one-hump travelling-wave solutions computed with the BE (resp. WIBL model) in solid (resp. dashed) lines for S = 1, Ma = 0, Re = 2.0667 and Ka = 3375 and wavenumbers: (a) $k = 0.0256$, (b) $k = 0.0169$, (c) $k = 0.0128$, (d) $k = 0.0084$. The closed flow condition was imposed.

Figure 5. Bifurcation diagram showing as solid lines families of one-hump wave solutions for various Re computed with the BE with S = 1, Ma = 0, Ka = 2950 and the closed flow condition. $A = (h_{\max} - h_{\min})/h_{\rm N}$ is the reduced wave amplitude. The dashed lines are the branches computed with the WIBL model for Re = 2, 3, 4 and 5. Asterisks and crosses indicate saddle-node bifurcations, the loci of which are followed through the parameter space in figure 6. IP: Intersection Point like in figure 3.

Figure 6. Stability diagram computed with the BE (same parameters as for figure 5). The solid line is the neutral curve $k_{\rm c}$. The Nusselt flat film is stable for $k > k_c$. The dashed line is the absence-of-solution boundary separating zones of stationary solutions (on the left) and of absence of one-hump solution (on the right). The dotted line is the same boundary for two-hump solutions ($n = 2$). The circles mark out the finite-time blow-up boundary obtained by Oron & Gottlieb (2002). $\mathrm{Re}_{\rm h}^*$ and $\mathrm{Re}_{\rm c}^*$ indicate the Reynolds numbers at which homoclines blow up and at which all the linearly unstable modes blow up, respectively. The asterisks and crosses correspond to the saddle-node bifurcation points as shown also in figure 5. The inset zooms in on the parameter range where the Hopf bifurcation becomes subcritical.

Figure 7. Stability diagram in the $(k, \mathcal{R})$–plane for a vertically falling, isothermal film, *i.e.* $\mathcal{C} = \mathcal{M} = 0$. The solid line is the neutral stability curve. The dashed (resp. dot-dashed) line is the blow-up boundary corresponding to the closed (resp. open) flow condition. The dotted line is the boundary where the amplitude of solutions of the BE exceed by about 10% the one of the WIBL model. The inset zooms in on the blow-up boundary in the vicinity of $\mathcal{R}_{\rm c}^*|_{\rm OP}$.

Figure 8. Stability diagram in the $(\mathcal{C}, \mathcal{R})$–plane for an isothermal film, *i.e.* $\mathcal{M} = 0$. The solid line is the neutral stability curve. The different regions from the left to the right are: **s**, the linearly stable region; **u**, the linearly unstable region where the BE gives bounded solutions in the whole range of unstable wavenumbers $k_{\rm c} > k > 0$; $\mathbf{u}_k|_{\rm CL}$, the linearly unstable region where the BE gives bounded solutions only in the range $k_{\rm c} > k > k^*$ when the closed flow condition is enforced; $\mathbf{u}_k|_{\rm OP}$, the same when the open flow condition is enforced; **b**, the region where all the linearly unstable modes are unbounded and yield finite-time blow-up. The circle represents a saddle-node bifurcation point found by Pumir

et al. (1983) with numerical simulations for $\beta = 11.3°$ and We $= 3000$. The plus sign corresponds to parameter of simulations by Joo *et al.* (1991). The dot-dashed lines are the loci of the reduced parameters corresponding to fixed inclination angle and fluid properties when the flow rate (or Reynolds number) is varied.

Figure 9. Stability diagram in the $(\mathcal{MB}, \mathcal{R})$–plane for a vertically falling film, *i.e.* $\mathcal{C} = 0$. Line styles and small letters are like in figure 8.

Figure 10. Stability diagram in the $(k, \mathcal{R})$–plane for a vertically falling film, *i.e.* $\mathcal{C} = 0$ and different values of $\mathcal{MB} = 0, 0.25, 0.5, 0.75$ and 1. The dotted lines are the corresponding neutral curves k_c and the dashed lines are the blow-up boundaries obtained with the closed flow condition. The dot-dashed lines are a selection of the blow-up boundaries obtained with the open flow condition. The inset shows bifurcation diagrams for $\mathcal{MB} = 0.5$ and $\mathcal{R} = 1.8$ (resp. Re $= 5$) with the closed (resp. open) flow condition, where the thick lines are computed with the BE and the thin lines with the WIBL model.

Figure 11. Maximum real part of the growth rate $\max(s_r)$ of disturbances and corresponding detuning parameter $\varsigma_{\max}$, versus wavenumber of stationary solutions of the BE (thick lines) and the WIBL model (thin lines). The solid (resp. dashed) lines correspond to closed (resp. open) flow. The letter "c" indicates the neutral mode at k_c and the asterisk indicates the solution at the blow-up boundary, *i.e.* for k^*. The calculations are made for a vertically falling and isothermal film, *i.e.* $\mathcal{C} = \mathcal{M} = 0$.

Figure 12. Time simulation starting from two periods of a stationary solution of the BE for $\mathcal{R} = 1.5$ and $k = 0.5$, put into a periodic domain of size 8π. A noise of amplitude 10^{-3} is added at $t = 0$. The main plot represents the time series of the film thickness recorded at the point $\xi = 7\pi$. The upper insets show, respectively, the two travelling-wave solutions at $t \approx 100$ and the coalesced wave at $t \approx 850$. The lower inset gives a zoom on a part of the time series showing oscillatory mode.

Figure 13. Space-time plot showing the evolution of a solution of the Benney equation (4.1) for $\mathcal{R} = 0.9$ in the vertical and isothermal case, *i.e.* $\mathcal{C} = \mathcal{M} = 0$. The film thickness is plotted at regular time intervals. The flow is open and oriented from left to right. A periodic forcing with noise is imposed at $x = 0$.

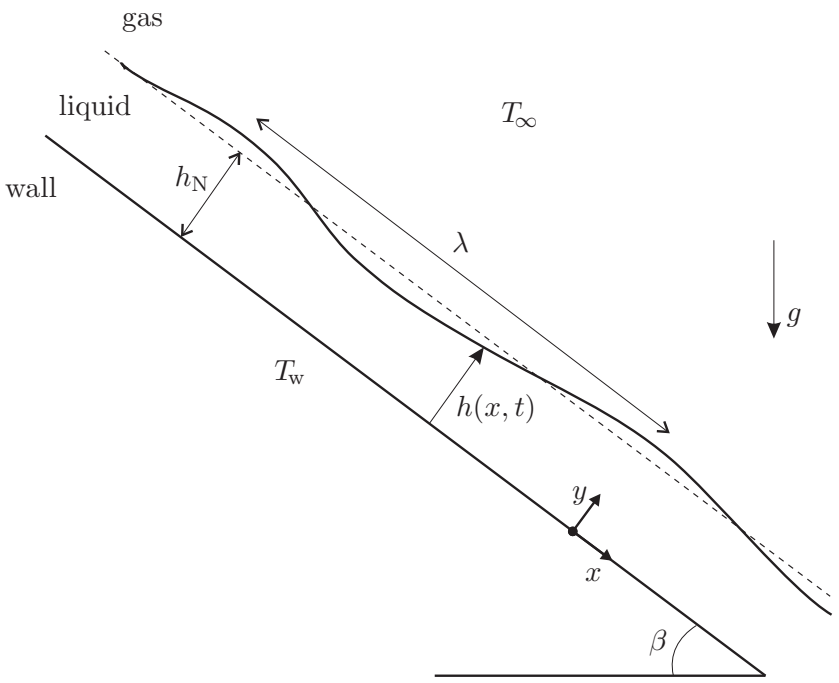

FIGURE 1. Scheid *et al.* , J. Fluid Mech.

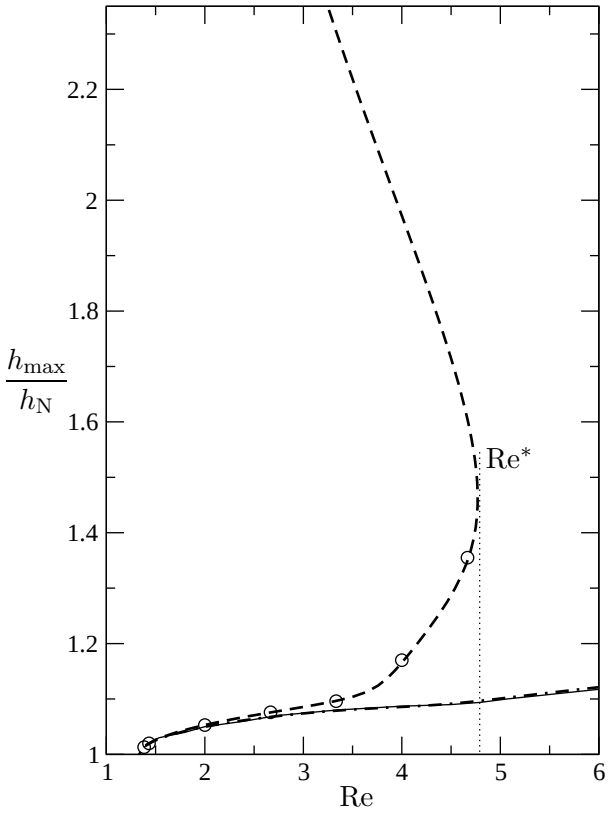

FIGURE 2. Scheid *et al.* , J. Fluid Mech.

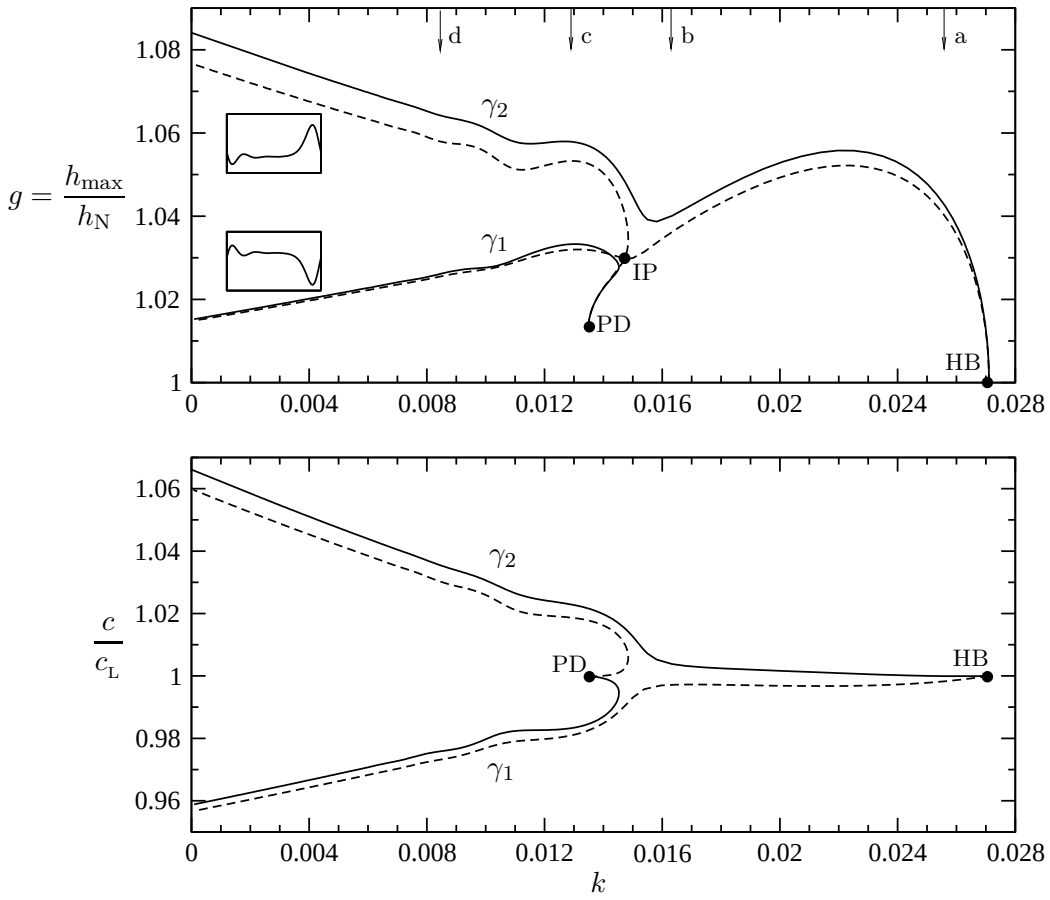

FIGURE 3. Scheid *et al.* , J. Fluid Mech.

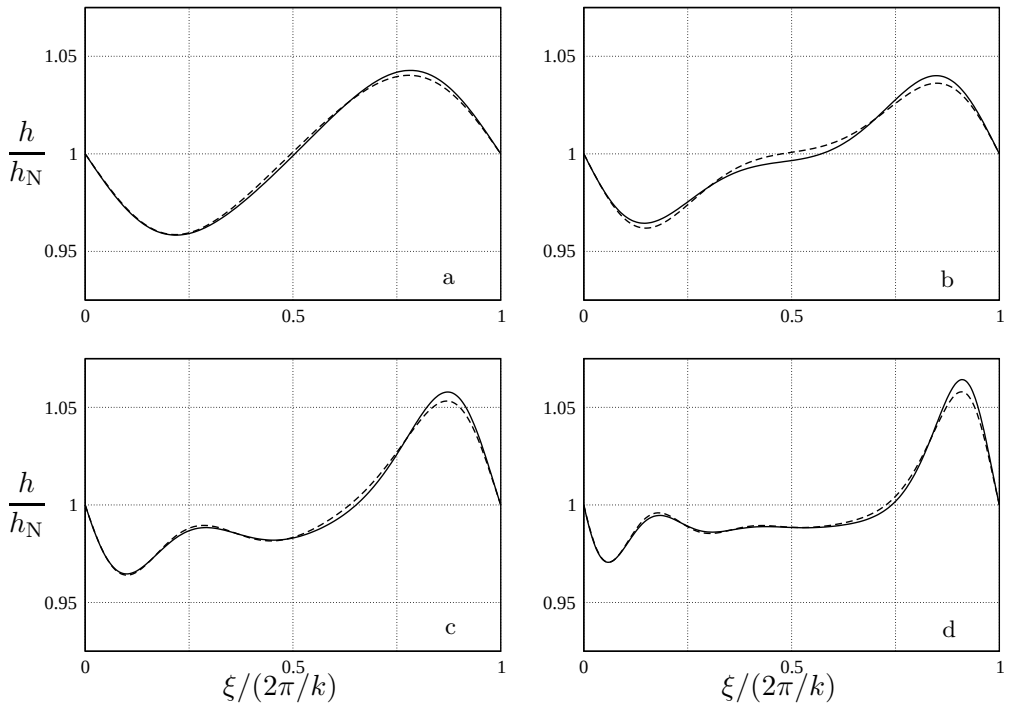

FIGURE 4. Scheid *et al.* , J. Fluid Mech.

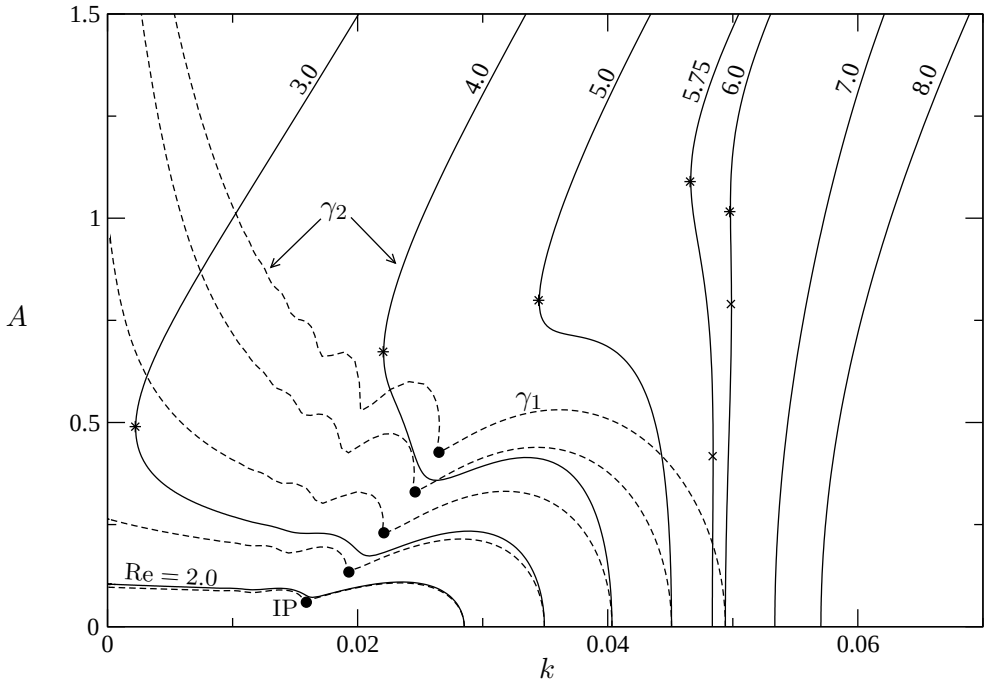

FIGURE 5. Scheid *et al.* , J. Fluid Mech.

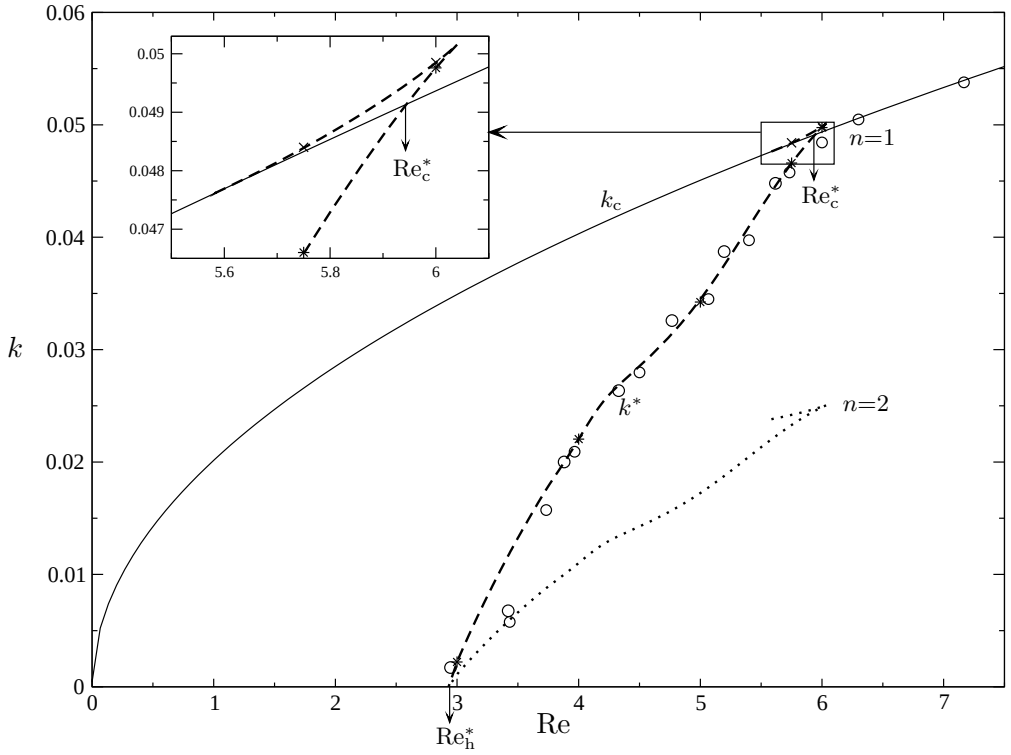

FIGURE 6. Scheid *et al.* , J. Fluid Mech.

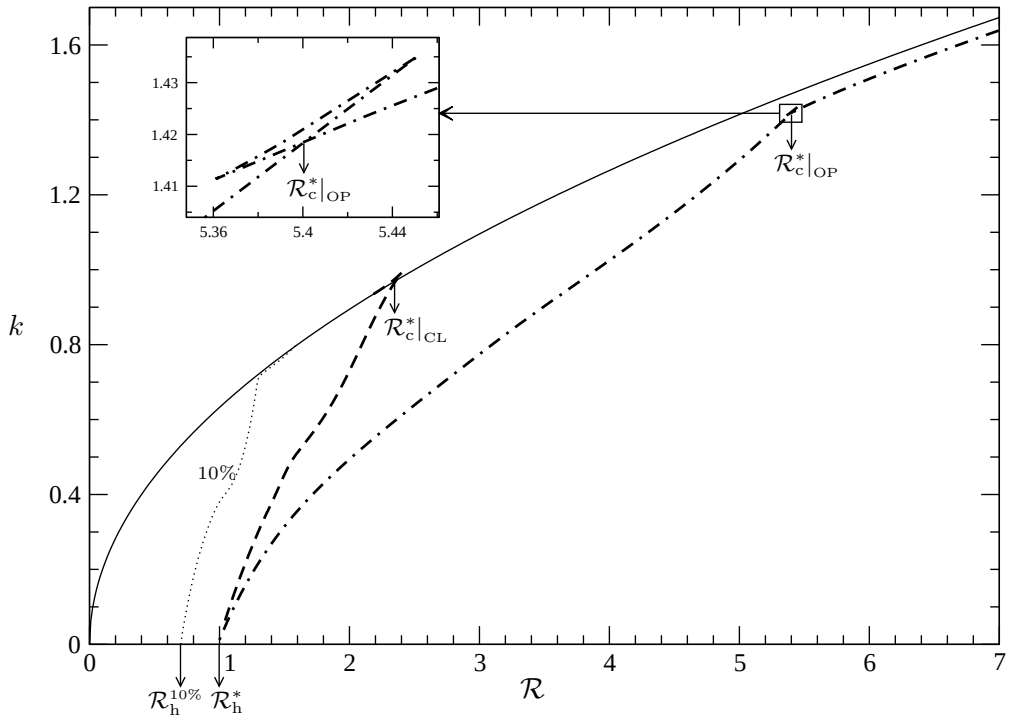

FIGURE 7. Scheid *et al.* , J. Fluid Mech.

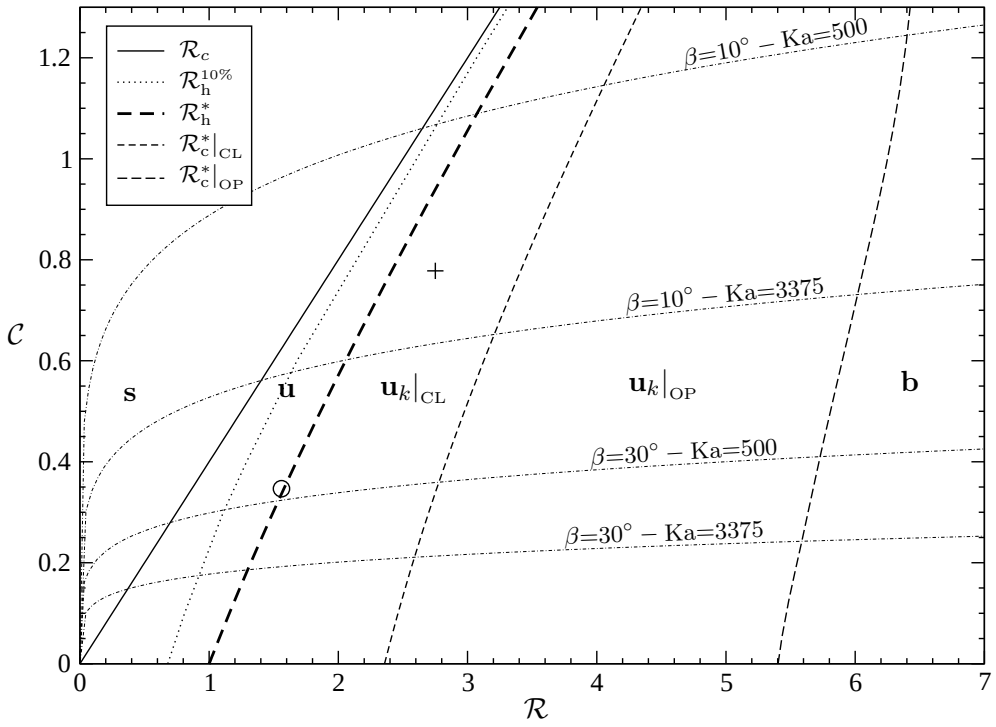

FIGURE 8. Scheid *et al.* , J. Fluid Mech.

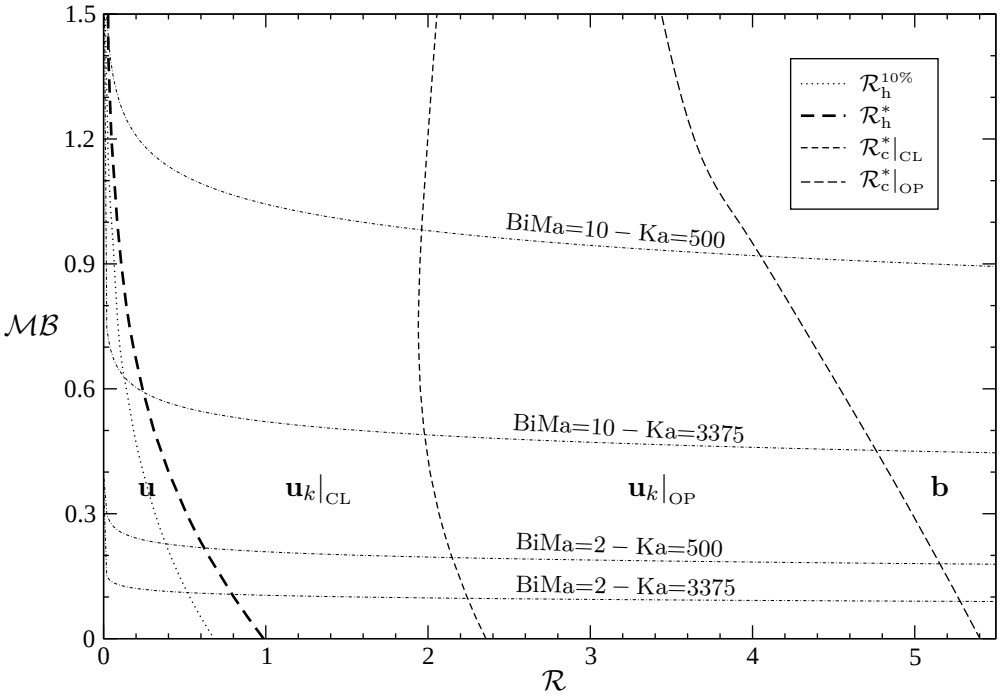

FIGURE 9. Scheid *et al.* , J. Fluid Mech.

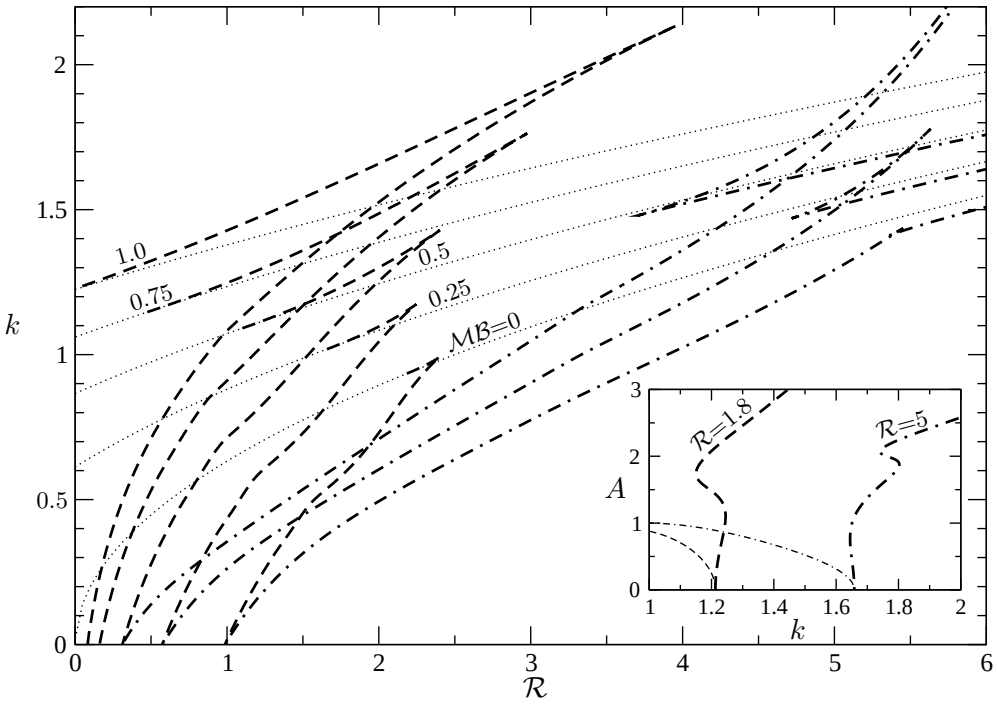

FIGURE 10. Scheid *et al.* , J. Fluid Mech.

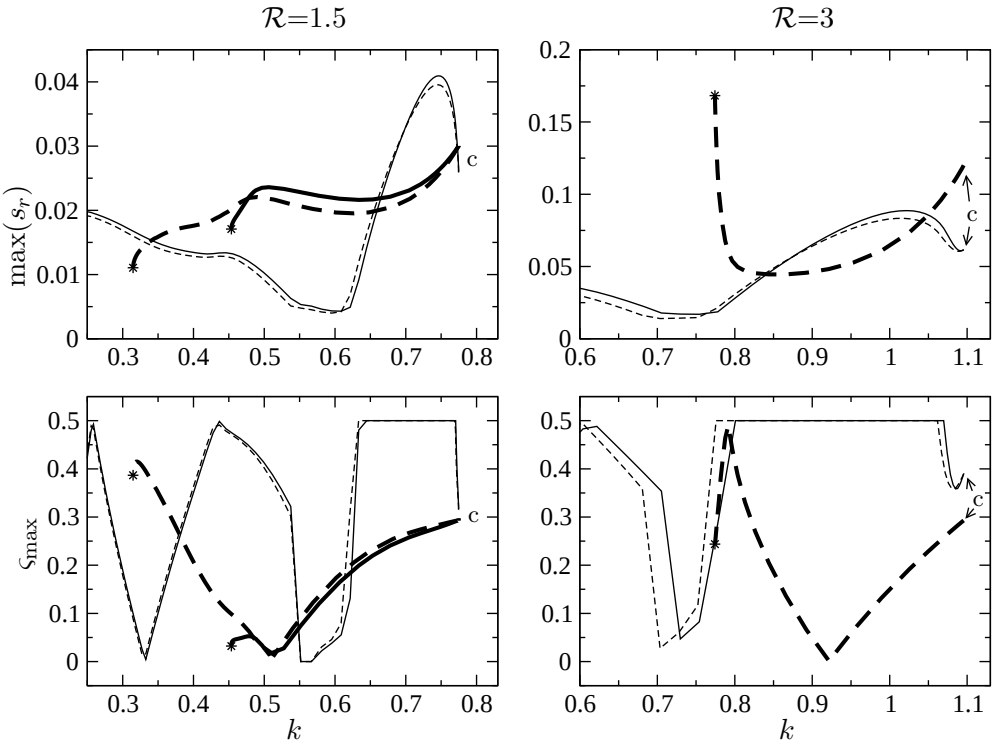

FIGURE 11. Scheid *et al.* , J. Fluid Mech.

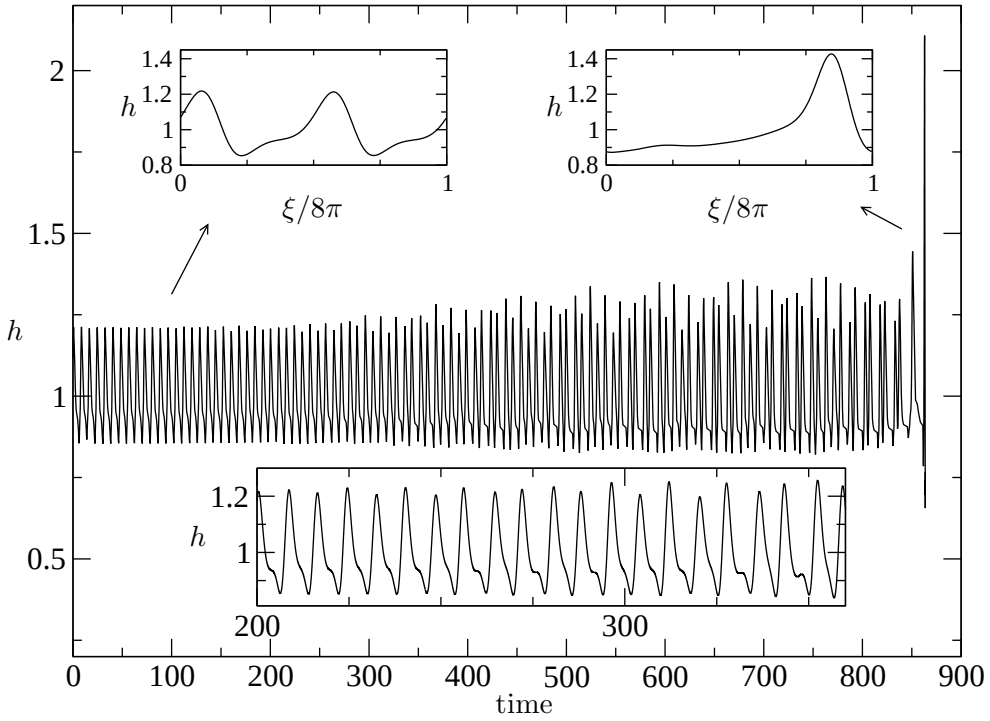

FIGURE 12. Scheid *et al.* , J. Fluid Mech.

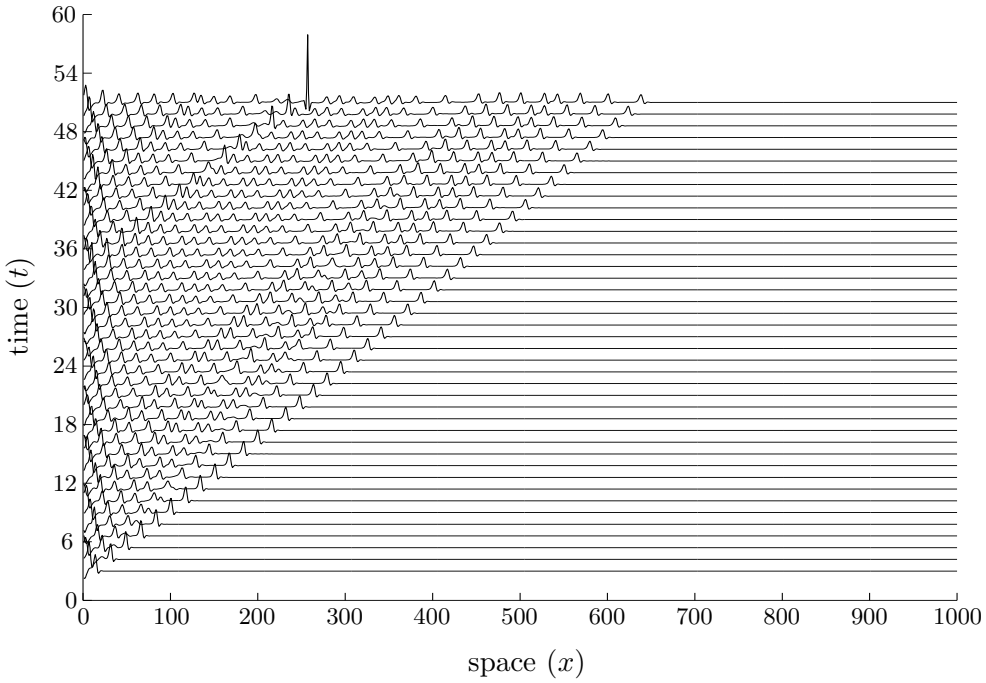

FIGURE 13. Scheid *et al.* , J. Fluid Mech.